Journal of Colloid and Interface Science 646 (2023) 413–425

Contents lists available at ScienceDirect

Journal of Colloid And Interface Science

journal homepage: www.elsevier.com/locate/jcis

Immobilization of *Agaricus bisporus* Polyphenol Oxidase 4 on mesoporous silica: Towards mimicking key enzymatic processes in peat soils

Claudia Iriarte-Mesa [a,b], Matthias Pretzler [c], Cornelia von Baeckmann [a,d], Hanspeter Kählig [e], Regina Krachler [f], Annette Rompel [c,*], Freddy Kleitz [a,*]

[a] Department of Inorganic Chemistry – Functional Materials, Faculty of Chemistry, University of Vienna, Währinger Str. 42, 1090 Vienna, Austria
[b] Vienna Doctoral School in Chemistry (DoSChem), University of Vienna, Währinger Str. 42, 1090 Vienna, Austria
[c] Universität Wien, Fakultät für Chemie, Institut für Biophysikalische Chemie, Josef-Holaubek-Platz 2, 1090 Vienna, Austria; www.bpc.univie.ac.at
[d] Catalan Institute of Nanoscience and Nanotechnology (ICN2), CSIC, and Barcelona Institute of Science and Technology, Campus UAB, Bellaterra, 08193 Barcelona, Spain
[e] Department of Organic Chemistry, Faculty of Chemistry, University of Vienna, Währinger Str. 38, 1090 Vienna, Austria
[f] Department of Inorganic Chemistry, Faculty of Chemistry, University of Vienna, Währinger Str. 42, 1090 Vienna, Austria

GRAPHICAL ABSTRACT

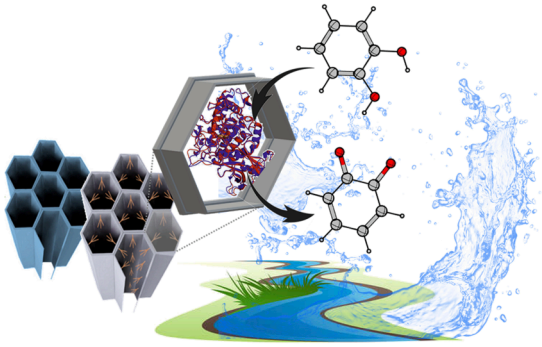

ARTICLE INFO

Keywords:
Tyrosinase
Mesoporous silica

ABSTRACT

Hypothesis: The use of immobilized enzyme-type biocatalysts to mimic specific processes in soil can be considered one of the most promising alternatives to overcome the difficulties behind the structural elucidation of riverine humic-derived iron-complexes. Herein, we propose that the immobilization of the functional mushroom

Abbreviations: ***Ab*PPO4**, *Agaricus bisporus* Polyphenol Oxidase 4; **APTS**, 3-aminopropyltriethoxysilane; **ATR-FTIR**, Attenuated total reflectance Fourier-transform infrared spectroscopy; **BET**, Brunauer-Emmet-Teller; **CP**, Cross-polarization; **DSC**, Differential scanning calorimetry; **EA**, Enzymatic activity; **L-DOPA**, 3,4-dihydroxy-L-phenylalanine; **MAS NMR**, Solid-state magic angle spinning nuclear magnetic resonance spectroscopy; **MS**, Mass spectrometry; **NLDFT**, Non-local density functional theory; **Pluronic P123**, Poly(ethylene glycol)-*block*-poly(propylene glycol)-*block*-poly(-ethylene glycol); **PPO**, Polyphenol oxidase; **PSD**, Pore size distribution; **SAHL**, Small aquatic humic ligand; **SBA-15**, Santa Barbara Amorphous type material #15; **SBA-15-NH_2**, APTS-modified SBA-15; **SBA-15-NH_2-Tyr**, *Ab*PPO4 loaded on APTS-functionalized silica; **SBA-15-Tyr**, *Ab*PPO4 loaded on non-functionalized silica; **SDS**, Sodium *n*-dodecyl sulfate; **TBC**, 4-*tert*-butylcatechol; **TEM**, Transmission electron microscopy; **TEOS**, Tetraethyl orthosilicate; **TGA**, Thermogravimetric analysis; **UHPLC**, Ultra-high-performance liquid chromatography.

* Corresponding authors at: Department of Inorganic Chemistry – Functional Materials, Faculty of Chemistry, University of Vienna, Währinger Str. 42, 1090 Vienna, Austria. (F Kleitz). Universität Wien, Fakultät für Chemie, Institut für Biophysikalische Chemie, Josef-Holaubek-Platz 2, 1090 Vienna, Austria. (A Rompel).
E-mail addresses: annette.rompel@univie.ac.at (A. Rompel), freddy.kleitz@univie.ac.at (F. Kleitz).

https://doi.org/10.1016/j.jcis.2023.04.158
Received 7 March 2023; Received in revised form 24 April 2023; Accepted 28 April 2023
Available online 1 May 2023

Enzyme adsorption
Biocatalysis
Phenol oxidation
SBA-15

tyrosinase, *Agaricus bisporus* Polyphenol Oxidase 4 (*Ab*PPO4) on mesoporous SBA-15-type silica could contribute to the study of small aquatic humic ligands such as phenols.

Experiments: The silica support was functionalized with amino-groups in order to investigate the impact of surface charge on the tyrosinase loading efficiency as well as on the catalytic performance of adsorbed *Ab*PPO4. The oxidation of various phenols was catalyzed by the *Ab*PPO4-loaded bioconjugates, yielding high levels of conversion and confirming the retention of enzyme activity after immobilization. The structures of the oxidized products were elucidated by integrating chromatographic and spectroscopic techniques. We also evaluated the stability of the immobilized enzyme over a wide range of pH values, temperatures, storage-times and sequential catalytic cycles.

Findings: This is the first report where the latent *Ab*PPO4 is confined within silica mesopores. The improved catalytic performance of the adsorbed *Ab*PPO4 shows the potential use of these silica-based mesoporous biocatalysts for the preparation of a column-type bioreactor for *in situ* identification of soil samples.

1. Introduction

Iron plays a crucial role in the maintenance of marine ecosystems as it is involved in regulating ocean carbon equilibria and biogeochemical cycles.[1,2] Complexation with biogenic ligands present in seawater increases iron solubility and ensures a life-sustaining concentration.[3–5] Small aquatic humic ligands (SAHLs) are inherently iron-containing compounds that play a key role in reducing the iron limitation of phytoplankton growth in the marine environment, thereby enhancing the marine biological carbon pump, a key process for capturing CO_2 on a global scale.[6] SAHLs have recently been shown to be the most important group of iron-bearing humic substances in peat-affected rivers.[7] However, up to now, little is known about the molecular structures of these iron-chelating ligands, due to their heterogeneity, low overall concentrations and various limitations associated with the structural analysis of humic substances.[8,9]

Low-molecular-weight phenolic compounds are exceptionally abundant in peat soils and can be converted into multidentate Fe-binding SAHLs due to the activity of polyphenol oxidases (PPOs) produced by soil bacteria.[10,11] PPOs are type 3 copper-containing enzymes requiring O_2 for their catalytic transformation of phenolic substances.[12,13] PPOs catalyze two different enzymatic reactions (Scheme 1), the *ortho*-hydroxylation and subsequent oxidation of monophenols to *o*-quinones (monophenolase, cresolase activity, EC 1.14.18.1) and the oxidation of catechols to *o*-quinones (diphenolase, catecholase activity, EC 1.10.3.1).[14,15] The reaction products undergo many secondary reactions, both with each other and with other substances (Scheme S2).[16,17] Hence, it is an important task to identify the products collected from soils *in situ*.

To overcome the difficulties behind the structural elucidation of iron complexes from river humus, attempts to immobilize peat-soil derived PPOs have gained increasing interest.[18–22] Studies on enzyme immobilization on different supports *via* a variety of routes have revealed that enzyme entrapment can increase its stability and decrease denaturation by protein unfolding.[18] Some of the biocatalysts produced are now used commercially at industrial scale, e.g., for the synthesis of L-aspartic acid, the production of acrylamide from acrylonitrile, the production of 6-aminopenicillanic acid from native penicillins and the production of fructose from starch.[23,24]

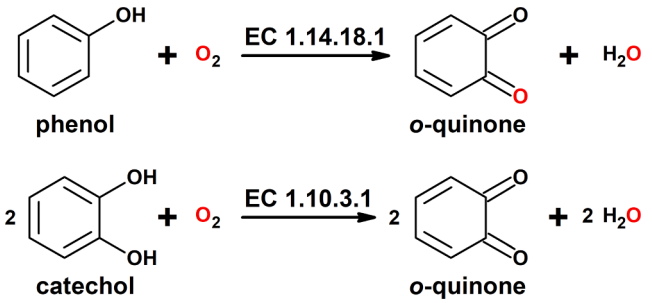

Scheme 1. *o*-Hydroxylation of monophenols and oxidation of catechols by polyphenol oxidases.

The immobilization of enzymes in ordered mesoporous materials has been studied for almost two decades and these have proven to be excellent supports to host enzymes.[24–27] Mesoporous materials possess suitable porosity and have been used successfully to encapsulate a variety of enzymes and other biomolecules.[28] In particular, robust mesoporous silica (pore size between 2 and 50 nm) can be easily prepared by a combination of templating (using surfactants) and inorganic sol–gel processes, generally under aqueous conditions.[29] The presence of surface silanol groups (Si-OH) allows interactions with enzymes and the grafting of a wide variety of functionalities through coupling reactions with organosilanes.[30–32] Ordered mesoporous silica of the SBA-15-type family represents an excellent starting point for the adsorption and immobilization of polyphenol oxidases.[33–36] These silica materials usually have a high surface area ($\geq$800-1000 $m^2 \cdot g^{-1}$) providing many adsorption sites, a high pore volume (>1 $cm^3 \cdot g^{-1}$) and large pore diameter (6–12 nm) for the enzyme to penetrate.[35] The morphology and dimensions of the particles can be tuned [37,38] and the materials can be fabricated into monolithic objects if required.[39,40].

To develop an accurate model for the formation of iron-chelating ligands, we focused on the immobilization of a functional mushroom tyrosinase, *Agaricus bisporus* Polyphenol Oxidase 4 (*Ab*PPO4, 65 kDa) on mesoporous SBA-15. *Ab*PPO4 was heterologously expressed by a reproducible protocol that provides large quantities of the tyrosinase, free of isoenzyme admixtures and side-activities commonly present in commercial preparations isolated from mushrooms.[14] *Ab*PPO4 was applied as the latent form of the enzyme containing the tyrosinase domain responsible for the catalytic activity as well as the C-terminal domain that blocks substrate access to the active site. Activation was effected by addition of the anionic detergent sodium *n*-dodecyl sulfate (SDS).[12] *Ab*PPO4 was incorporated into the silica mesopores *via* liquid adsorption, which ensures easy preparation of the biocatalysts, low production costs, and the possibility of reloading the support.[28] The influence of the surface charge of the silica support on the loading efficiency of *Ab*PPO4 was evaluated by functionalization of SBA-15 with a positively charged aminosilane, 3-aminopropyltriethoxysilane (APTS), introduced through a post-grafting strategy.[41] The prepared *Ab*PPO4-based catalysts were successfully used for the catalytic oxidation of phenolic compounds, confirming the advantages of enzyme immobilization and confinement, such as improved stability and reusability. The use of these biocatalysts would allow the design of an optimized bioreactor that mimics specific processes in peat soils, leading to the study of humic-derived iron complexes.

2. Materials and methods

2.1. Materials

Tetraethyl orthosilicate (TEOS, 98%), anhydrous toluene (99.8%), sodium *n*-dodecyl sulfate (SDS, 99%), sodium (meta)periodate ($NaIO_4$,

≥99.8%) and poly(ethylene glycol)-*block*-poly(propylene glycol)-*block*-poly(-ethylene glycol) (Pluronic P123, $EO_{20}PO_{70}EO_{20}$, $M_n \sim 5800$) were purchased from Sigma Aldrich. Trisodium citrate dihydrate (99%), sodium hydroxide (NaOH, 1.0 N standardized solution), sodium chloride (NaCl, 99.0%), 3-aminopropyltriethoxysilane (APTS, 98%), citric acid anhydrous (>99.5%), L-tyrosine (99%), tyramine (>98%), dopamine hydrochloride (99%), 3,4-dihydroxy-L-phenylalanine (L-DOPA, >98%) and sodium hydrogen phosphate, (Na_2HPO_4, anhydrous, 99%) were purchased from Alfa Aesar. Hydrochloric acid (HCl, 37%) and 4-*tert*-butylcatechol (TBC, 99%) were purchased from VWR Chemicals and Fisher Scientific, respectively. The functional mushroom tyrosinase, *Agaricus bisporus* Polyphenol Oxidase 4 (*Ab*PPO4, 65 kDa) was heterologously expressed at the Department of Biophysical Chemistry of the University of Vienna, providing a single isoform of tyrosinase (Figure S1).[14]

2.2. Synthesis and functionalization of mesoporous SBA-15

SBA-15 silica used as enzyme support was synthesized following the procedure described by Guillet-Nicolas *et al.*[37] Precisely, 8 g of Pluronic P123 were first dissolved in a solution of concentrated HCl (4.46 g, 37%) and distilled water (146.25 g). This mixture was stirred at 35 °C until complete dissolution of the polymer. When P123 was completely dissolved, 13 g of tetraethyl orthosilicate (TEOS, Sigma-Aldrich, 98%) were added to the mixture and incubated under stirring at 35 °C. After 24 h, the mixture was heated to 100 °C in a convection oven (Binder, Germany) and kept under static conditions at 100 °C for 48 h. The hot solution was vacuum filtered without washing (Whatman® filter paper, Grade 541, diameter 110 mm) and dried for 2 h at 100 °C and then overnight at 140 °C. Pluronic P123 was removed by solvent extraction for 2 h in a solution of 200 mL of ethanol (96%) with two drops of concentrated HCl (37%) followed by calcination at 550 °C under air.

SBA-15 was functionalized with APTS by modifying the protocol reported by von Baeckmann *et al.*[41] Typically, 500 mg of calcined SBA-15 were degassed overnight at 150 °C and then dispersed in 80 mL of anhydrous toluene under stirring and argon atmosphere at 115 °C. After 3 h, 0.6 mL of APTS (5 mmol·g^{-1} of SBA-15) were added and the reaction was stirred overnight at 115 °C. The amino-functionalized SBA-15 (SBA-15-NH_2) was recovered by centrifugation (9 000 × g, 20 min), washed once with toluene, twice with ethanol and dried at 80 °C overnight.

2.3. Loading of AbPPO4 on mesoporous silica

Agaricus bisporus Polyphenol Oxidase 4 (*Ab*PPO4, 65 kDa) was introduced into the pores of SBA-15 and SBA-15-NH_2 through physical adsorption. First, enzyme solutions (concentration range from 1 μM to 100 μM) in Tris-HCl buffer (50 mM Tris-HCl, 150 mM NaCl, pH 7.1) were prepared from a concentrated solution of *Ab*PPO4 (20 g·L^{-1}). For obtaining the adsorption isotherms, 15 mg of SBA-15 or SBA-15-NH_2 were slowly shaken in 2.5 mL of these enzyme solutions for 48 h at 4 °C, followed by centrifugation (9 000 × g, 30 min). The enzyme-loaded materials (SBA-15-Tyr or SBA-15-NH_2-Tyr) were lyophilized and stored at 4 °C for further evaluation. The supernatants were collected in order to determine the remaining enzyme concentration *via* UV/Vis. For the phenol oxidation experiments and enzyme stability determinations, the loading protocol was scaled up using 50 mg of SBA-15 or SBA-15-NH_2 and a total concentration of *Ab*PPO4 of 5 g·L^{-1} that ensured maximum loading efficiency.

2.4. Enzymatic activity determination

To verify that the enzyme preserved its activity once it is adsorbed on the silica supports, 10 mg of the enzyme-loaded silica (SBA-15 or SBA-15-NH_2) were suspended in 720 μL sodium citrate buffer at pH 6.8 (50 mM) followed by the addition of 30 μL SDS (100 mM) for activation of the latent enzyme [14] and 750 μL L-tyrosine (2 mM). Already after 3 min, a pronounced change in color was observed. After 15 min, the suspensions were centrifuged (11 770 × g, 2 min) and the supernatants analyzed *via* UV/Vis, getting the maximum absorbance at 475 nm (L-dopachrome). For the enzymatic activity determination of the control (free *Ab*PPO4), L-tyrosine (750 μL, 2 mM), sodium citrate buffer (670 μL, 50 mM) and SDS (30 μL, 100 mM) were mixed in a quartz cuvette. Afterwards, 50 μL of free *Ab*PPO4 (0.67 g·L^{-1}) were added and the mixture was quickly shaken. The absorbance was measured at 475 nm (ε_{475} = 3600 $M^{-1}\cdot cm^{-1}$) [14] every 5 s during 5 min. A line was fitted to the data using Origin Pro 2019 (OriginLab Corp., USA) software, and the slope was directly correlated to the enzymatic activity of the free *Ab*PPO4. The solid enzyme-loaded catalysts SBA-15-Tyr and SBA-15-NH_2-Tyr, as well as the free *Ab*PPO4 (20 g·L^{-1}, 50 mM sodium citrate buffer, pH 6.8), were stored at 4 °C for stability determination over time. The residual enzymatic activity was determined once a week during the first month and later after 24 weeks and one-year storage.

2.5. Oxidation of phenols by free and adsorbed AbPPO4

*Ab*PPO4-adsorbed silica catalysts (SBA-15-Tyr or SBA-15-NH_2-Tyr) were dispersed in a mixture containing citrate buffer (2.4 mL, 50 mM, pH 6.8), SDS (100 μL, 100 mM) and 2.5 mL of the phenolic substrate (dopamine, tyramine, L-tyrosine or TBC, 2 mM). The dispersions were placed on a mechanical shaker at room temperature for 20 min, taking 100 μL aliquots every minute for the first 10 min and at the end of the experiment. The enzyme present in the sample aliquots was inactivated by adding HCl (1 M, 500 μL) and citrate buffer (400 μL, 50 mM, pH 6.8). These acidic samples (pH = 3) were filtered (Puradisc™ Polyvinylidene Difluoride Syringe Filters, diameter 4 mm) and then aliquots of 200 μL were taken and diluted with water (800 μL) prior to HPLC/MS analysis. The experiment was also performed with the free *Ab*PPO4 (control) using 200 μL of enzyme solution (0.5 mg·mL^{-1} for the reaction with tyramine or L-tyrosine, and 12.5 μg·mL^{-1} when the enzyme was added to the catechols dopamine or TBC). The conversion values (%) at specific time-points (t) were expressed as a function of the substrate concentration in each sample (c_t) with respect to the initial concentration (c_0) before the addition of the free or adsorbed *Ab*PPO4 ($t = 0\ min$):

$$Conversion(\%) = \left(1 - \frac{c_t}{c_0}\right) \times 100 \quad (1)$$

2.6. Adsorption of phenolic compounds and oxidized products within silica pores

Adsorption of oxidized phenolic compounds on mesoporous silica was carried out by dispersing calcined SBA-15 or SBA-15-NH_2 (5 mg) in 2 mL of a mixture containing the phenols tested (dopamine, DOPA or TBC; 2 mM; 1 mL), $NaIO_4$ (100 μL, 200 mM), citrate buffer (860 μL, 50 mM, pH 6.8) and SDS (40 μL, 200 mM). The dispersions were placed in a mechanical rocker for 5 or 20 min at room temperature and then, the solid was centrifuged (11770 × g, 2 min) and the supernatants analyzed *via* UV/Vis. The isolated solids were washed continuously with SDS (200 mM)/citrate buffer (50 mM) (1:24 *v/v*) or water, collecting the supernatants for UV/Vis analysis. The silica materials were lyophilized and stored at 4 °C for further evaluation.

2.7. Influence of SDS concentration on the enzyme activity of immobilized AbPPO4

The behavior of the confined enzyme with respect to the SDS concentration was carried out by dispersing the *Ab*PPO4-loaded SBA-15 (SBA-15-Tyr, 2 mg, 38 wt% of *Ab*PPO4) in citrate buffer (50 mM, pH 6.8) and varying the volume of SDS (10 mM) added to the mixture. The volumes of citrate buffer (50 mM, pH 6.8) and SDS (10 mM) were adjusted such that the final concentration of SDS after adding L-tyrosine

(750 μL, 2 mM) was 0.1, 0.25, 0.5, 1.0, 2.0, and 4 mM in the total reaction volume of 1.5 mL. The experiment was also carried out in the absence of SDS. The enzyme activity tests were performed as described in section 2.4.

2.8. Thermal stability of AbPPO4

For the thermal stability determinations, six different dispersions of SBA-15-Tyr (2 mg, 38 wt% of adsorbed *Ab*PPO4) in sodium citrate buffer (720 μL, 50 mM; pH 6.8) were prepared and slowly stirred (80 rpm) at 10, 30, 40, 50, 60 and 70 °C for 1 h. Once the samples were at room temperature, the residual enzymatic activities were tested (section 2.4) after adding SDS (30 μL, 100 mM) and L-tyrosine (750 μL, 2 mM). The thermal stability of free *Ab*PPO4 (50 mL, 0.67 $g{\cdot}L^{-1}$) was determined following the same procedure and used as control.

2.9. pH-stability of free and confined AbPPO4

The stability of the adsorbed-*Ab*PPO4 was determined in a pH range from 2 to 8. First, SBA-15-Tyr (2 mg, 38 wt% of loaded *Ab*PPO4) was dispersed in 1 mL of McIlvaine buffers (pH = 2.2, 3, 5, 7, and 8) and placed in an incubator (4 °C) under gentle stirring (80 rpm) for 1 h. The McIlvaine buffers were prepared from the mixture of Na_2HPO_4 (0.2 M) and citric acid (0.1 M) at different proportions and subsequent pH adjusting with HCl (0.25 M) or NaOH (0.2 M).[42,43] The catalysts were isolated by centrifugation (11770 × g, 2 min) and the respective enzyme activity tests were performed as described in section 2.4. The pH stability of the free enzyme was carried out under the same conditions and used as control. The native *Ab*PPO4 (60 μL; 0.67 $g{\cdot}L^{-1}$) was mixed with 940 μL of McIlvaine buffers and stirred for 1 h at 4 °C. Then, 25 μL of these solutions were transferred to a quartz cuvette containing a mixture of citrate buffer (695 μL, 50 mM, pH 6.8) and SDS (30 μL, 100 mM). Enzyme activity was determined by following the oxidation of L-tyrosine (2 mM; 750 μL) for 5 min by UV/Vis spectroscopy (λ = 475 nm). The enzyme activities of free and confined *Ab*PPO4 (SBA-15-Tyr) were also measured after dispersing the respective samples for 1 h at 4 °C in citrate buffer (50 mM; pH 6.8) and were used as reference.

2.10. Reusability of adsorbed AbPPO4 on mesoporous silica

The catalyst SBA-15-Tyr (5 mg, 38 wt% of adsorbed *Ab*PPO4) was dispersed in sodium citrate buffer (720 μL, 50 mM, pH 6.8) followed by addition of SDS (30 μL, 100 mM) and L-tyrosine (750 μL, 2 mM). After 15 min, the suspensions were centrifuged (11 770 × g, 2 min) and the supernatants analyzed *via* UV/Vis, getting the maximum absorbance at 475 nm (L-dopachrome). The solid was redispersed in citrate buffer and vortexed for 3 min before the next catalytic reaction with L-tyrosine. This procedure was repeated for 16 consecutive cycles.

2.11. Materials characterization

N_2-physisorption isotherms measurements were carried out at −196 °C (77 K) using an Autosorb-iQ3 sorption analyzer (Anton Paar, Boynton Beach, USA). Before the analysis, calcined SBA-15 and APTS-modified SBA-15 (SBA-15-NH_2) were outgassed overnight at 150 °C and 80 °C, respectively. The enzyme loaded samples were outgassed at 35 °C for 20 h prior to analysis. The surface area (S_{BET}) was determined using the Brunauer-Emmet-Teller (BET) method [44] in the relative pressure range 0.05–0.3 P/P_o. The pore size distributions (PSD) were estimated using the non-local density functional theory (NLDFT) method on the equilibrium branch, considering an amorphous SiO_2 (oxide) surface and a cylindrical pore model. The calculations were carried out using the ASiQwin 5.2 software provided by Anton Paar Quantatech Inc.[37] Transmission electron microscopy (TEM) images were collected with a Philips CM200 microscope at an accelerating voltage of 200 kV, using suspensions of SBA-15 and SBA-15-NH_2 in EtOH deposited on a carbon-coated copper grid. Low-angle diffraction data was recorded on a PANalytical Empyrean diffractometer (Malvern PANalytical, United Kingdom) in a transmission geometry (Focusing mirror) using Cu $K\alpha_{1+2}$ radiation operated at a voltage of 45 kV, a tube current of 40 mA and with a fixed divergence slit of 0.76 mm. Measurements were performed in the continuous mode with a step size for 2θ of 0.013° and a data collection time per step of 50 s for the transmission mode. Thermogravimetric (TGA) and differential scanning calorimetry (DSC) analyses were executed using a Netzsch STA-449 F3 Jupiter instrument from 25 to 800 °C under airflow of 20 $mL{\cdot}min^{-1}$ as carrier gas with a heating rate of 10 $°C{\cdot}min^{-1}$. The mass losses (%) were estimated in the temperature range from 150 to 700 °C. The zeta-potential measurements of SBA-15 and SBA-15-NH_2 were performed with a Malvern Nano Zetasizer ZS. To guarantee correct calibration before zeta-potential measurements, a standard suspension (carboxylate modified polystyrene latex microspheres) with a zeta-potential of − 40 (±6) mV was measured. Aqueous suspensions of the materials (0.7 $mg{\cdot}mL^{-1}$) were obtained by performing three cycles of vortex shaking (10 min) and ultrasonic bath treatment (30 min). The supernatants were then analyzed to obtain zeta-potential values. Solid-state magic angle spinning nuclear magnetic resonance spectroscopy (MAS NMR) was performed on a Bruker Avance NEO 500 wide bore system (Bruker BioSpin, Rheinstetten, Germany). A 4 mm triple resonance magic angle spinning (MAS) probe was used. Cross-polarization (CP) was employed using a ramped contact pulse thereby sweeping the proton radio frequency field from 50 to 100%. For ^{29}Si, the resonance frequency was 99.38 MHz, the MAS spinning speed was 8 kHz, and the CP contact time was 5 ms. The resonance frequency for ^{13}C NMR was 125.78 MHz, the MAS rotor spinning was set to 14 kHz, and the CP contact time to 3 ms. During acquisition, ^{1}H was high-power decoupled using SPINAL with 64 phase permutations.[41] Chemical shifts (δ) are reported in ppm and referenced externally for ^{13}C to adamantane by setting its low field signal to 38.48 ppm. For ^{29}Si the shifts were referenced externally to sodium trimethylsilylpropane sulfonate (DSS) by setting the signal to 0 ppm. ^{1}H-liquid NMR spectra were recorded at a resonance frequency of 700.40 MHz on a Bruker Avance III HD 700 spectrometer (Bruker BioSpin, Rheinstetten, Germany) equipped with a helium cooled quadruple cryoprobe. All measurements were done at a temperature of 25 °C using a mixture of 5% D_2O/95% H_2O as solvent. The water signal was suppressed by presaturation and for referencing the carrier frequency was set to 4.67 ppm. Attenuated total reflectance Fourier-transformed infrared (ATR-FTIR) spectra were recorded using a Bruker Vertex 70 FTIR spectrometer equipped with the Specac Golden Gate ATR accessory. The spectra were obtained from the acquisition of 72 scans at 4 cm^{-1} resolution in the range of 4000 to 500 cm^{-1}. Before each measurement, a background spectrum was collected, gathered from the acquisition of 72 scans at 4 cm^{-1} resolution. UV/Vis absorption spectra were collected on an Onda UV-30 SCAN spectrophotometer at room temperature (25 °C). All samples were analyzed in 1 cm quartz cuvettes. The quantification of phenolic compounds and oxidized products was performed using a Vanquish Horizon ultra-high-performance liquid chromatography (UHPLC) system (Thermo Fisher Scientific, Germering, Germany) coupled to a LTQ Orbitrap Velos mass spectrometer (Thermo Fisher Scientific, Bremen, Germany) equipped with an electrospray ion source with the voltage set to 3 kV and an ion transfer capillary temperature of 380 °C. Separation of analytes was carried out on a C-18 analytical column Acclaim 120 (2.1 × 150 mm, 3 μm, Thermo Fisher Scientific) at a flow rate of 0.4 $mL{\cdot}min^{-1}$. The column oven temperature was set to 30 °C and the injection volume was 5 μL. The mobile phases were A: H_2O (0.1% (v/v) formic acid) and B: ACN (0.1% (v/v) formic acid). A linear gradient method was applied as follow: 0.0 – 8.0 min: 5–53% B, 8.0–8.5 min: 53–95% B, 8.5–12.5 min: 95% B, 12.5–13.0 min: 95–5% B and re-equilibration was done until 17 min. The full-scan mass spectra (MS) were acquired in positive and negative ion mode in the range of 80 – 500 *m/z* at a resolution of 60000. Samples containing TBC were measured in negative ion mode in order to detect the phenolic

substrate. The correspondent oxidized product TBC_{ox}, was detected in positive ion mode like the rest of the analyzed compounds. SDS-PAGE was performed using the classical discontinuous buffer system (stacking and separating gel) and the single running buffer according to the Laemmli-protocol.[45] The gel used was cast with a linear gradient of 8%-15% acrylamide in the separating gel and 5% acryalmide in the stacking gel. Electrophoresis was performed for 30 min at 10 $V{\cdot}cm^{-1}$ and 90 min at 15 $V{\cdot}cm^{-1}$ using the Bio-Rad Mini-PROTEAN Tetra Vertical Electrophoresis Cell. Gel staining with Coomassie brilliant blue G-250 and Al^{3+} was carried out according to the protocol of Kang *et al.*[46] The destained gel was then photographed using a Bio-Rad Gel Doc XR Imaging System.

3. Results and discussion

3.1. Synthesis and functionalization of mesoporous SBA-15

The SBA-15 used as enzyme support in this study was synthesized according to established protocols that yield tunable and high-quality silica materials.[47] Materials with different pore sizes could be obtained by varying the temperature of the hydrothermal treatment during the synthesis.[38] Based on the literature, the synthesis conditions of SBA-15 were chosen to ensure the formation of pores large enough for enzyme encapsulation and keeping it confined within the mesoporous structure. The obtained SBA-15 was functionalized with a positively charged amino-silane, 3-aminopropyltriethoxysilane (APTS), through a classical post-grafting strategy.[41]

The mesostructured ordering of SBA-15 and SBA-15-NH_2 was verified by low-angle XRD measurements (Fig. S2a). Three well-resolved diffraction peaks were observed in the corresponding diffractograms and were indexed as 100, 110, and 200 reflections, typical of two-dimensional (2D) hexagonal mesostructures with a pore symmetry of *p6mm*. The positions of three diffraction peaks for SBA-15-NH_2 were similar to its all-silica precursor SBA-15, indicative of the retention of the ordered pore structure after surface functionalization. The TEM images of both materials (Fig. S2b) revealed the periodic alignment of the channel-like pores, which is in agreement with the low-angle XRD data.

Both materials exhibit a typical type IVa isotherm with a sharp H1 hysteresis and a capillary condensation at a relative pressure (P/P_0) range of 0.6–0.8 (Fig. S2c). NLDFT pore size distributions were fairly narrow for both materials (Fig. S2d, Table S2), which is expected for mesoporous silica with well-defined and uniform mesopores.[38,48] From the NLDFT pore size distributions, it was found that the SBA-15 had a pore size of 9.1 nm. Upon modification, the pore size of the SBA-15-NH_2 was reduced to 8.1 nm. Likewise, both the specific surface area and the pore volume decreased after functionalization, from 743 to 403 $m^2{\cdot}g^{-1}$ and from 1.34 to 0.76 $cm^3{\cdot}g^{-1}$, respectively (Table S2). Such decreases are consistent with the introduction of the organosilane on the pore surface, without major pore blocking, and still enough space in the pores of the functionalized silica for the later encapsulation of the *Ab*PPO4 enzyme with a homogenous distribution within the mesopores (Figure S3). Surface functionalization of SBA-15 was also confirmed by thermogravimetric analysis (TGA), from a weight loss of 8.9 wt% (SBA-15-NH_2) attributed to the thermal decomposition of the organic moieties on the functionalized silica between 150 and 700 °C (Fig. S4a). The solid-state ^{29}Si CP/MAS NMR spectrum of SBA-15-NH_2 (Figure S5) revealed the T^2 and T^3 signals, which indicates successful chemical modification of the SBA-15 silica surface. No T^0-species were observed, confirming the absence of non-covalently attached APTS (Table S1). Moreover, in the solid-state ^{13}C CP/MAS NMR spectrum of SBA-15-NH_2 (Fig. 1a), three resonance signals were observed at 42.9, 25.5 and 9.0 ppm, attributed to the carbons of the silane propyl chain, located in alpha, beta and gamma positions of the amine, respectively.

Additional confirmation of the successful surface modification of the SBA-15 was obtained through Zeta-potential measurements in nanopure water (Fig. 1b), whereas the amino-modified silica SBA-15-NH_2 exhibited a positive surface charge over the pH range tested, in contrast to its all-silica precursor SBA-15. The Zeta-potential of both materials was also measured in Tris-HCl buffer (50 mM, pH = 7.4), the same medium in which the loading of the *Ab*PPO4 enzyme was performed later. The Zeta-potential values obtained in the buffer medium were −10.3 (±0.6) mV and +13.9 (±0.6) mV for SBA-15 and SBA-15-NH_2, respectively. Considering that *Ab*PPO4 is negatively charged under these conditions,[49] this enabled the evaluation of the effect of surface charge on the support–enzyme interactions and the catalytic performance of the immobilized enzyme.

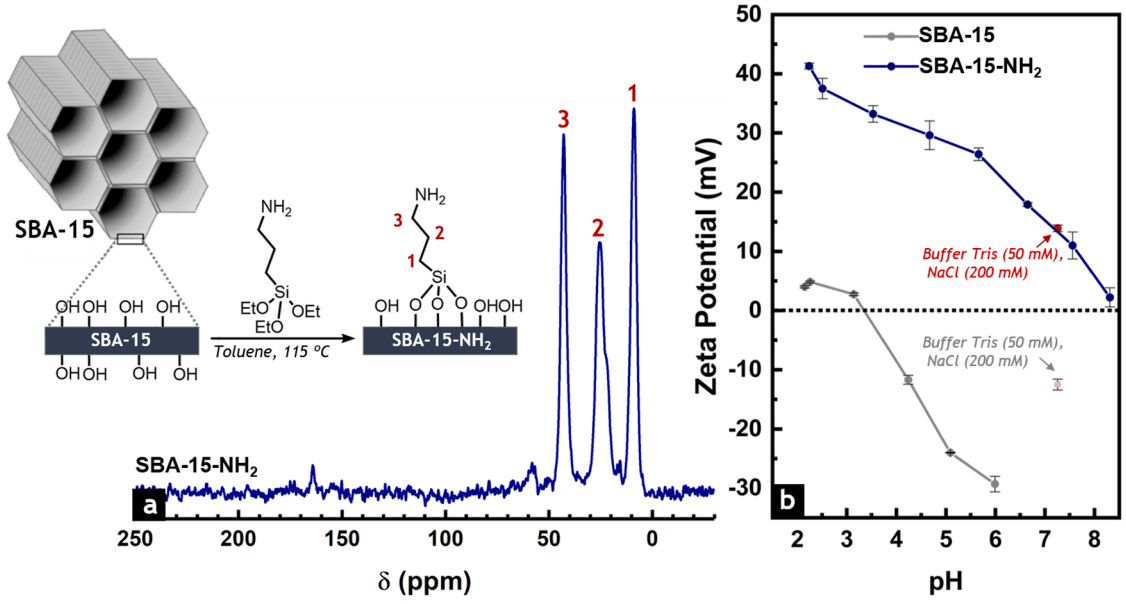

Fig. 1. (a) Solid-state ^{13}C CP/NMR spectra of APTS-functionalized silica SBA-15-NH_2 (b) Zeta-potential of SBA-15 (grey) and SBA-15-NH_2 (blue), measured over the pH range 2–8 as well as in the buffer used for enzyme loading (50 mM Tris-HCl, pH = 7.4; red circle and dot). (For interpretation of the references to color in this figure legend, the reader is referred to the web version of this article.)

3.2. *Ab*PPO4 adsorption and enzyme activity

The polyphenol oxidase *Ab*PPO4 was inserted into silica pores by physical adsorption. Equilibrium enzyme adsorption isotherms were obtained by preparing solutions at different defined total concentrations of *Ab*PPO4 that were put in contact with SBA-15 and SBA-15-NH_2 in Tris-HCl buffer (pH 7.2) for 48 h at 4 °C. The supernatants obtained after the enzyme loading were analyzed *via* UV/Vis in order to determine the remaining enzyme concentration (Figure S6). The enzyme quantification was performed following the band at 280 nm correspondent to the absorbance from tryptophan, phenylalanine and tyrosine residues of the *Ab*PPO4.[50] Using this absorption, the amount of *Ab*PPO4 in the supernatant was calculated. Subtraction of that value from the total applied amount of *Ab*PPO4 provided the adsorbed amount of *Ab*PPO4. The data shown in Fig. 2a indicates a steep linear increase of adsorption with increasing enzyme concentration until reaching a plateau, which corresponds to the maximum amount of *Ab*PPO4 absorbed on SBA-15 (7.2 μmol·$g^{-1}$of silica) and SBA-15-NH_2 (3.2 μmol·g^{-1} of silica). TGA of the enzyme-loaded materials revealed an increase in mass loss from 2.2 to 38 wt%, consistent with increasing equilibrium adsorbed enzyme concentrations in the isotherm (Fig. 2b, Figure S6, b-c), with the highest mass loss for the highest concentrations of immobilized enzyme, due to the plateau regime (38 wt% and 16 wt% for enzyme-loaded SBA-15 and SBA-15-NH_2, respectively). The lower adsorption capacity of SBA-15-NH_2 in comparison to SBA-15 was attributed to its lower pore size and overall lower porosity, which prevented the adsorption of higher amounts of *Ab*PPO4. Although the introduction of amino-functionalities changed the external surface charge of SBA-15 to positive values as observed in Fig. 1b, favoring the electrostatic interaction of SBA-15-NH_2 with the negatively charged *Ab*PPO4, the presence of the hydrophobic carbon chain of the APTS could also have decreased the polarity of the grafted silica compared to the non-functionalized support.[41] This could additionally limit the amount of enzyme loaded on SBA-15-NH_2-Tyr.

Furthermore, N_2-physisorption analysis at 77 K performed on loaded samples, SBA-15-Tyr and SBA-15-NH_2-Tyr (Figure S7; Table S2) showed a substantial decrease in pore volume and surface area of the materials after the enzyme adsorption, leading to the assumption that most of the enzyme was indeed located within the pores. This could also be corroborated by low angle-XRD measurements (Fig. 2c). In the diffractograms of the *Ab*PPO4-loaded SBA-15-Tyr samples, the diffraction peaks indexed as 100, 110, and 200 reflections were observed as a result of retention of ordered structure after enzyme loading, as expected. Moreover, their systematic broadening and decrease in intensity with increasing loaded enzyme concentration indicated that the pores are progressively filled by *Ab*PPO4 and its confinement in the silica mesopores.

The same trend was observed for the low angle-patterns of different SBA-15-NH_2-Tyr samples (Figure S8), which suggested rather uniform enzyme confinement within the amino-functionalized mesopores. To rule out the possible presence of adsorbed enzyme at the mouth of the mesopores due to the interaction of *Ab*PPO4 with amino groups of the external surface of SBA-15-NH_2, a physical mixture was prepared by adding a solution of *Ab*PPO4 (3.1 μmol·g^{-1} of silica) to SBA15-NH_2 before freeze-drying. Subsequently to the drying, the low angle-XRD analysis was performed and the intensity normalized relative to the silica amount. As observed in Figure S8, the intensity of the diffraction peaks of this sample (green dotted line) was similar to the control (SBA-15-NH_2, black dotted line) without enzyme. These results support the confinement of *Ab*PPO4 within the silica mesopores.

To verify that the tyrosinase preserved its catalytic performance throughout the immobilization process, enzymatic activity tests were performed following the oxidation of L-tyrosine (2 mM) by UV/Vis in citrate buffer at pH 6.8 (Fig. 3).

When testing the tyrosinase-loaded silicas (SBA-15-Tyr and SBA-15-NH_2-Tyr) containing different amounts of adsorbed *Ab*PPO4, a clear color change was observed already after 3 min interaction with L-tyrosine (Fig. 3, inserts) due to the formation of the oxidation product L-dopachrome (Fig. 3, Figure S11). After 15 min, the suspensions were centrifuged and the supernatants analysed *via* UV/Vis spectroscopy. The spectra shown in Fig. 3 correspond to mixtures of 200 μL of supernatants solutions with 800 μL of citrate buffer. The enzyme concentration dependence of the reaction was clearly observed since the highest amount of L-dopachrome (absorption band centred at 475 nm) could be detected for the highest concentrations of immobilized enzyme for both SBA-15-Tyr (38 wt%, Solution 7, Fig. 3a) and SBA-15-NH_2-Tyr (16 wt%, Solution 6, Fig. 3b). These observations provided a strong first indication that the latent enzyme retained its activity after immobilization. The enzyme activity test was also carried out using a solution of free *Ab*PPO4 at the same maximum concentration of immobilized tyrosinase on SBA-15 (7.2 μmol·g^{-1} of SBA-15) and under the same conditions (solution labelled as T, Fig. 3a). The maximum absorption at 475 nm (Fig. 3a, dotted black line) was similar to the maximum absorbances obtained when the samples with the highest loaded amount of *Ab*PPO4 were tested. This constitutes strong evidence that the enzymatic activity of *Ab*PPO4 is not significantly affected when it is adsorbed on silica. For tyrosinase-loaded silica SBA-15-Tyr (7.2 μmol·g^{-1} of SBA-15), the enzymatic activity experiment was performed without the addition of

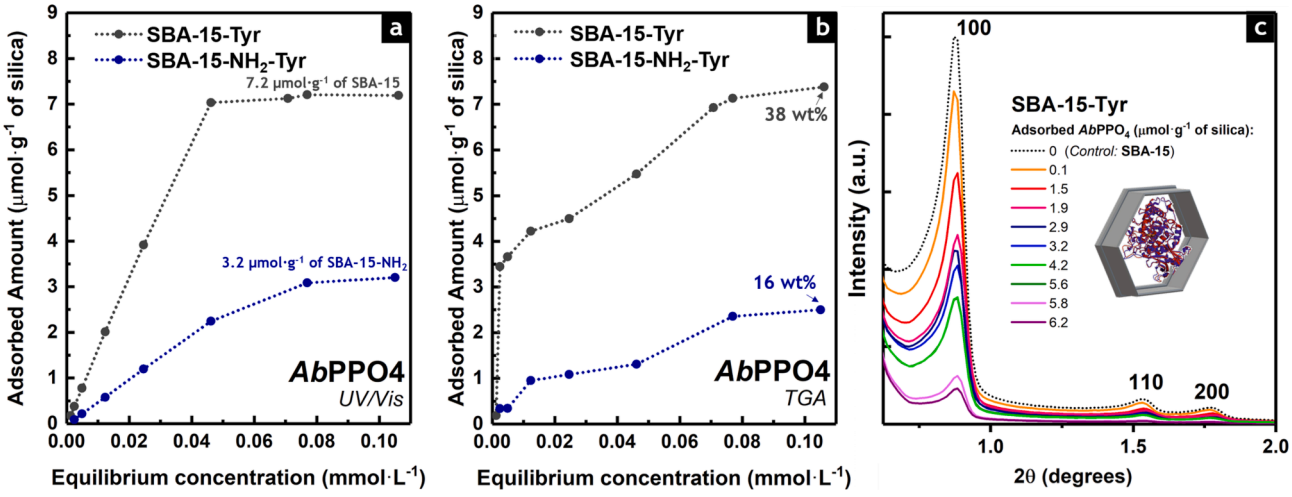

Fig. 2. Enzyme adsorption isotherms of SBA-15 and SBA-15-NH_2 silica at 4 °C obtained by (a) UV/Vis and (b) TGA. (c) Low-angle XRD patterns of the different tyrosinase-loaded samples on non-functionalized SBA-15 (SBA-15-Tyr). Scattering intensities were normalized with respect to the amount of silica in each sample.

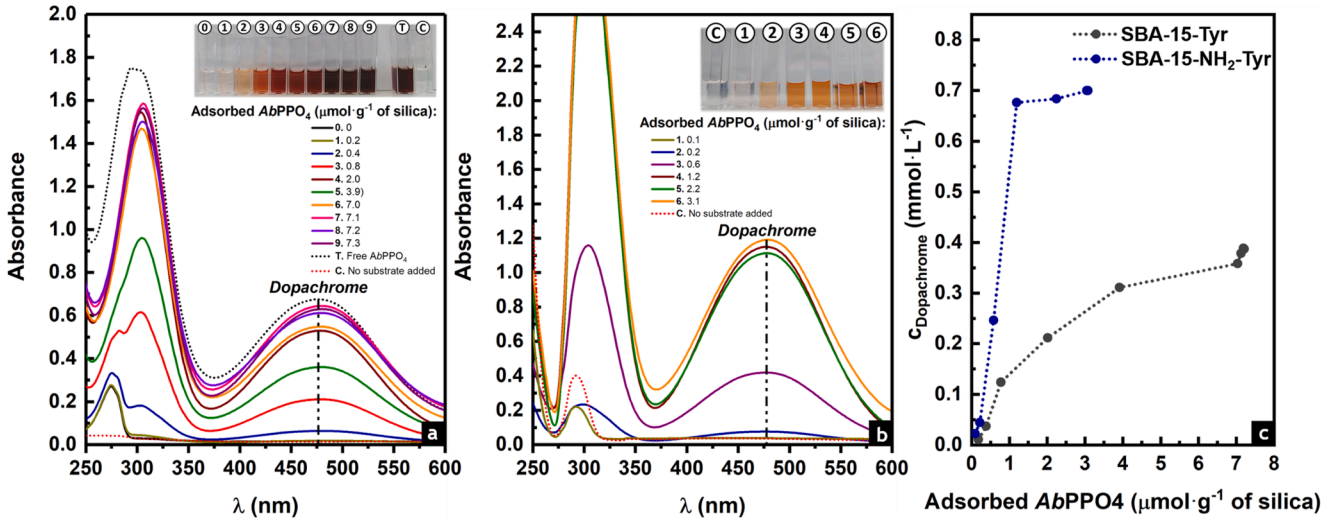

Fig. 3. UV/Vis spectra of the diluted supernatants (5 times dilution) after 15 min of reaction of L-tyrosine with (a) *Ab*PPO4-loaded SBA-15 silica and (b) *Ab*PPO4-loaded SBA-15-NH_2. *Inserts:* corresponding photo of the samples. (c) Concentration of L-dopachrome produced in the catalytic reaction as a function of concentration of *Ab*PPO4 loaded on SBA-15-Tyr (grey line) or SBA-15-NH_2-Tyr (blue line). (For interpretation of the references to color in this figure legend, the reader is referred to the web version of this article.)

substrate (Control, solution C) and no activity was observed in these conditions. The supernatant obtained after separating the solid was analysed *via* UV/Vis spectroscopy. The negligible adsorption observed at 280 nm (Fig. 3a, dotted red line) confirmed that the immobilized enzyme is not desorbed from silica during enzyme activity assays and hence the observed enzyme activity in the presence of substrate originates from the immobilized enzyme.

To further confirm that the immobilized *Ab*PPO4 is not released in solution from the silica support an additional leaching test was performed (Figure S9). The conditions for the enzymatic activity test were adjusted for SBA-15-Tyr but without adding substrate (L-tyrosine). The catalyst was shaken in the presence of citrate buffer and SDS, and after 15 min the solid was isolated by centrifugation. The negligible absorption observed at 280 nm in the supernatant suggested the absence of desorbed enzyme in solution (grey line), as previously described. After adding L-tyrosine (final concentration 1 mM), only the band at 275 nm corresponding to the absorbance from the added substrate was observed (blue line). However, after 15 min of interaction of the isolated solid with L-tyrosine, the mixture was centrifuged and the corresponding supernatant analyzed by UV/Vis. An intense absorption band at 475 nm was observed, indicating the oxidized product L-dopachrome (red line). The intensity of this band was similar to the control (dotted black line), *i.e.*, the same amount of SBA-15-Tyr where the enzyme activity was evaluated by adding L-tyrosine at the beginning of the experiment. These results confirm that the enzyme remains confined in the mesopores during the catalytic reaction.

From the enzymatic activity studies, it was possible to calculate the concentration of L-dopachrome produced after 15 min of reaction of L-tyrosine with the different catalysts obtained (Fig. 3c). The maximum concentration of L-dopachrome obtained (0.39 $mmol{\cdot}L^{-1}$ and 0.71 $mmol{\cdot}L^{-1}$ for the reaction catalysed by SBA-15-Tyr and SBA-15-NH_2-Tyr, respectively) was corresponding to the maximum amount of immobilized *Ab*PPO4 and showed an enhanced biocatalytic performance with respect to other tyrosinase-immobilized silica catalysts.[51–53] It should be noted here that the enzyme immobilized on SBA-15-NH_2 was able to produce higher concentrations of L-dopachrome in comparison with equivalent enzyme concentrations in SBA-15-Tyr. Although the adsorption capacity of SBA-15-NH_2 was lower than that of SBA-15, the immobilized *Ab*PPO4 on the amino-functionalized material showed better catalytic performance, possibly as a result of a more efficient interaction between the positively charged carrier and the immobilized tyrosinase in the pores.

3.3. Oxidation of phenolic compounds

The oxidation of L-tyrosine and other phenolic compounds (TBC, dopamine and tyramine) was followed individually by HPLC/MS using SBA-15-Tyr (38 wt% of latent *Ab*PPO4) and SBA-15-NH_2-Tyr (13.2 wt% of *Ab*PPO4), as represented in Scheme S1.

At different time-points of the reactions, 100 μL aliquots were taken and the reaction was stopped by acidifying the medium with HCl (0.1 M) to inactivate the enzyme (pH = 3). The samples were then centrifuged and filtered for subsequent HPLC/MS measurements. The MS analysis allowed elucidating the structure of the oxidized products and determining their relative proportion with respect to the initial concentration of the phenolic substrate (Fig. 4). For each phenolic compound studied, mixtures of several oxidation products were detected according to the gradual decrease in the relative abundance of the substrate (Scheme S2). For dopamine, L-tyrosine and tyramine, also intense signals corresponding to deamination ions $(M - 17)^+$ were detected as result of the NH_3-loss.[54]

Interestingly, upon oxidation of tyramine ($m/z = 138$), the product obtained as a result of *o*-hydroxylation of monophenol (dopamine, $m/z = 154$) seemed to stabilize and took longer to produce the corresponding dopachrome derivative ($m/z = 150$) when the reaction was catalyzed by confined *Ab*PPO4. When the free enzyme was used to catalyze the same reaction, the relative proportions of the dopamine intermediate were negligible and the major oxidation product was the dopachrome-derivative ($m/z = 150$), the same major product that was determined when the reaction was carried out with dopamine ($m/z = 154$) as the substrate. The corresponding *o*-quinone ($m/z = 152$), obtained from the oxidation of dopamine, could also be detected. The relative abundance of this *o*-quinone intermediate was the highest in the reactions catalyzed by the adsorbed enzyme (SBA-15-Tyr and SBA-15-NH_2-Tyr), suggesting the stabilization of the intermediate within the silica pores. In the case of the reactions with TBC, the substrate was detected in negative ion mode, in contrast to the other phenolic compounds investigated. No intermediate products were observed in positive ion mode during the oxidation of the catechol and the formation of the corresponding *o*-quinone ($m/z = 165$) was corroborated.

In the supernatants corresponding to reactions with L-tyrosine (m/z = 182), the monophenol hydroxylation product (DOPA, m/z = 198) and the correspondent dopaquinone (m/z = 196) were undetectable. The relative levels of dopachrome (m/z = 194) were very low. However, the product of the decarboxylation of dopachrome (m/z = 150) was found, as well as the product of the subsequent α-deprotonation (m/z = 148).

The dopachrome transformation through oxidation of L-tyrosine by SBA-15-Tyr, SBA-15-NH_2-Tyr and the free *Ab*PPO4 was followed by ^{1}H NMR over time (Figure S10). The formation of dopachrome in the early stages of the reaction was corroborated from the increase in the signal intensities at 6.5 ppm and 5.7 ppm. However, when the free *Ab*PPO4 was used for the catalysis, a gradual decrease in these signal intensities was observed after 10 min, and at the same time the signal at 6.3 ppm was increased (α-deprotonated derivative). The gradual decrease in dopachrome concentration was also observed during the oxidation by SBA-15-Tyr and SBA-15-NH_2-Tyr, but only after 35 min from the start of the reaction. These results suggested the stabilization of the dopachrome due to its adsorption within the silica pores, resulting in its slower transformation into the α-deprotonated product. Fig. 5 shows the conversion (%) obtained from the HPLC/MS measurements and calculated from the decrease in the initial concentrations of the phenolic substrates. For all phenolic compounds tested, conversions between 25% and 92% were achieved after 20 min of reaction, with similar and even improved biocatalytic performances compared to free *Ab*PPO4 (control).

Table 1 includes the specific enzyme activity values EA (U·mg^{-1}) obtained for each of the reactions studied. The EA was expressed as the amount of free or adsorbed *Ab*PPO4 that catalyzed the reaction of 1 μmol of substrate per minute (U), reported per mg of protein.[55] For each of the phenolic substrates studied, a considerable drop in the EA of the immobilized *Ab*PPO4 was observed when compared to the free enzyme, decreasing up to 30-fold for SBA-15-Tyr and 10-fold for SBA-15-NH_2-Tyr in the reactions with dopamine and TBC (catechols). In the catalytic reaction with tyramine, the EA decreased only 4-fold and 2-fold for SBA-15-Tyr and SBA-15-NH_2-Tyr, respectively. A similar catalytic performance was observed during the oxidation of L-tyrosine, where the EA of SBA-15-Tyr was 2-fold decreased relative to the free *Ab*PPO4, and was even enhanced (up to 20%) when the reaction was catalyzed by SBA-15-NH_2-Tyr. These results demonstrate the positive effect of the amino-functionalization of the silica support. Although for both SBA-15-Tyr and SBA-15-NH_2-Tyr it was verified that the enzyme is confined within the mesopores, *Ab*PPO4 loading on the amino-functional SBA-15 could result in more favorable orientation of the loaded enzyme, arising 3 times higher EA values for the amino-functionalized catalyst in comparison to SBA-15-Tyr, where the *Ab*PPO4 only interacts with the –OH moieties of the silanol groups of the non-functionalized support.

3.4. Adsorption of phenolic compounds and oxidized products within silica pores

The apparent drop in enzyme activity after immobilization has been previously reported, as well as the alteration of the conformation of the enzyme with respect to its native state.[56–58] Furthermore, the decrease in the enzymatic activity could also be attributed to the adsorption of the components of the buffer used for catalysis (*i.e.*, citrate and SDS) in the silica mesopores. This was corroborated by studying the adsorption of standard solutions of phenolic compounds on SBA-15 and SBA-15-NH_2. The studied compounds (dopamine$_{ox}$, DOPA$_{ox}$ and TBC$_{ox}$) were previously oxidized with sodium periodate and put in contact for 5 or 20 min with SBA-15 and SBA-15-NH_2, in the same conditions under which the enzyme activity studies were performed with the enzyme-loaded catalysts.

The mass losses (%) of the solid samples obtained after the adsorption were found between 20 wt% and 37 wt% (Fig. 6a). Those values were similar or even lower than those obtained for SBA-15 and SBA-15-NH_2 samples that did not interact with oxidized phenols but were prepared under the same conditions (control samples represented with grey

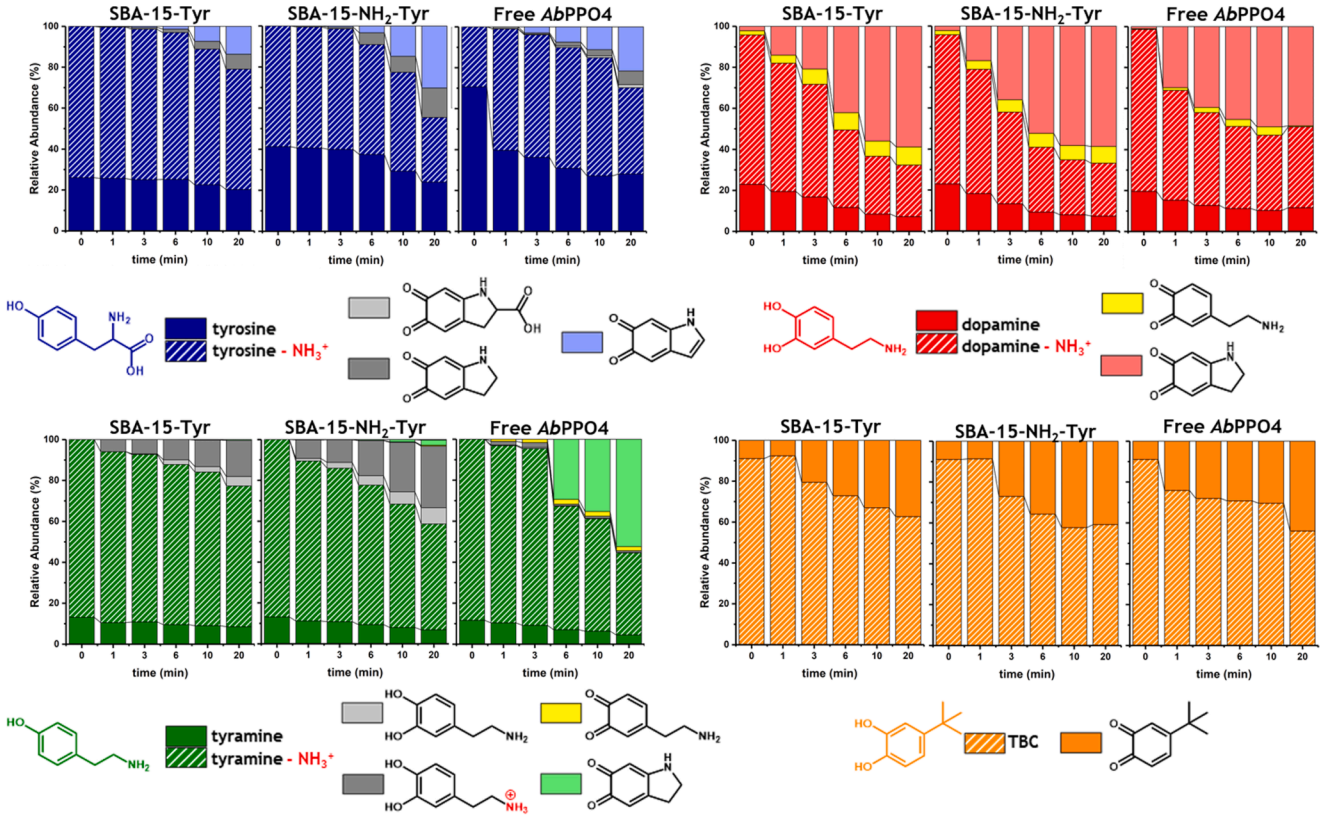

Fig. 4. MS characterization of the products obtained from the oxidation of phenolic compounds at different time periods in correlation with their respective proportion.

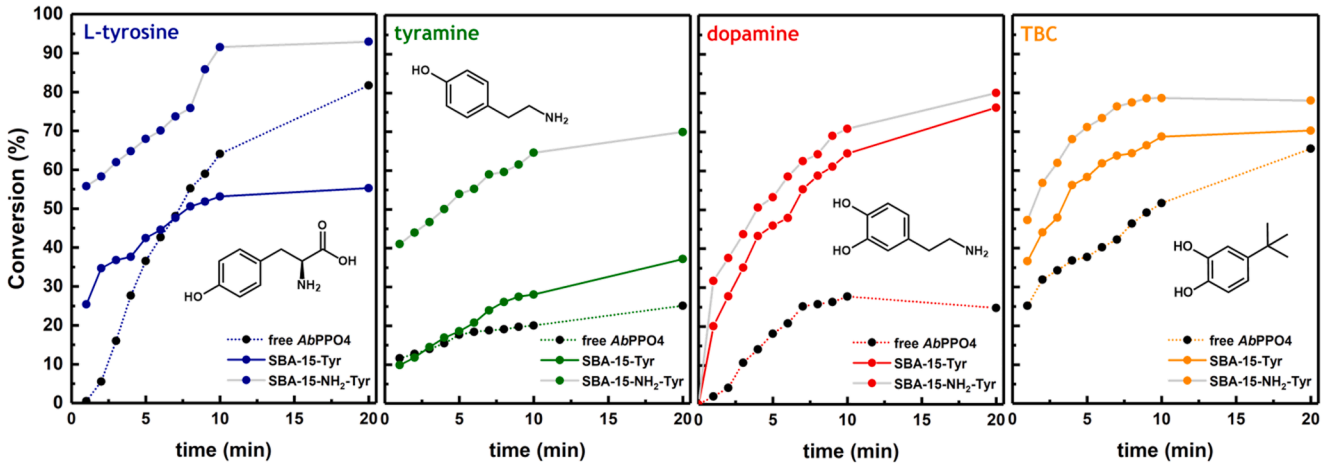

Fig. 5. Oxidation of phenolic compounds followed by HPLC/MS. The biocatalytic performances of *Ab*PPO4 loaded on non-functionalized SBA-15 (SBA-15-Tyr; 38 wt %) and on the APTS-modified silica (SBA-15-NH_2-Tyr; 13.2 wt%) were tested and compared with free *Ab*PPO4 (control).

Table 1
Reaction rate (μM·min^{-1}) and specific activity (U·mg^{-1}) of free and adsorbed *Ab*PPO4 during the oxidation of phenolic compounds.

Substrate	Catalyst	*Ab*PPO4 concentration (mg·L^{-1})	Reaction rate (μM·min^{-1})	EA (U·mg^{-1})
L-tyrosine	SBA-15-Tyr	131.9	25.0	0.19 (46.6%)
(1 mM)	SBA-15-NH_2-Tyr	59.7	29.2	0.49 (120.1%)
	free *Ab*PPO4 (Control)	20.0	8.2	0.41
tyramine	SBA-15-Tyr	134.5	22.7	0.17 (23.5%)
(1 mM)	SBA-15-NH_2-Tyr	61.6	26.4	0.43 (59.8%)
	free *Ab*PPO4 (Control)	20.0	14.3	0.72
dopamine	SBA-15-Tyr	134.5	374.4	2.78 (3.5%)
(1 mM)	SBA-15-NH_2-Tyr	59.4	476.1	8.01 (10.2%)
	free *Ab*PPO4 (Control)	0.5	39.3	78.6
TBC	SBA-15-Tyr	128.2	201.5	1.57 (3.2%)
(1 mM)	SBA-15-NH_2-Tyr	55.3	275.1	4.97 (10.2%)
	free *Ab*PPO4 (Control)	0.5	24.5	49.0

bars in Fig. 6). These results confirmed that most of the organic matter adsorbed here on the silica corresponds to the citrate buffer and/or SDS, which could block the pores, preventing the access of substrate molecules to the catalytic sites during the loaded-enzyme reaction, with a negative impact on the reaction rate and the apparent enzyme activity.

The UV/Vis spectra of the supernatants obtained after 20 min-interaction of dopamine$_{ox}$, DOPA$_{ox}$ and TBC$_{ox}$ with SBA-15 were similar to the spectra of standard solutions prepared under the same conditions but without adding silica (Figure S11). These results confirmed the negligible adsorption of oxidized phenols within silica pores. The significant decrease in the intensity of the adsorption maximum ($\lambda = 470$ nm, 468 nm and 400 nm for Dopamine$_{ox}$, DOPA$_{ox}$ and TBC$_{ox}$, respectively) compared to freshly prepared standards (Figure S11, black lines) was attributed to the low stability of these oxidized phenols due to overoxidation caused by the 10-fold excess of sodium periodate. In contrast, better defined maxima but of low intensity were observed in the spectra of the supernatants correspondent to the SBA-15-NH_2 samples, suggesting the possible adsorption and stabilization of the oxidized phenols.

The oxidation of L-tyrosine was also carried out using SBA-15-Tyr as catalyst but varying the SDS concentration (Figure S12) in order to study the influence of the surfactant adsorption on the catalytic performance. A gradual increase in the concentration of the dopachrome-derivative produced was observed when the SDS concentration increased up to 4 mM. This suggested that even when the anionic surfactant is adsorbed in the pores of the silica, its presence does not affect the reaction rates. Thus, despite that the adsorption of catechols is not ruled out (Fig. 7, insert), the major cause of the lower apparent enzymatic activity of SBA-15-Tyr and SBA-15-NH_2-Tyr compared to the free *Ab*PPO4 may be associated with excess of citrate adsorbed within silica pores.

The samples obtained after the interaction of SBA-15 and SBA-15-NH_2 with oxidized phenols were further analyzed using solid-state ^{13}C CP/MAS NMR, which confirmed the presence of citrate adsorbed in the silica pores (Fig. 7a). The signals corresponding to the citrate molecules were found in all the samples analysed at 177–185 ppm, 75 ppm and 42–46 ppm, and were maintained even after the sixth washing with the same medium in which the experiments were carried out (Fig. 7b).

Despite citrate being the compound mainly adsorbed in the pores of SBA-15 some weak signals in the sample washed with water after the adsorption of oxidized dopamine could be observed in the ^{13}C CP/MAS NMR spectra (Fig. 7b, insert). Additionally, the ATR-FTIR spectra of the samples obtained after the oxidation of L-tyrosine by SBA-15-Tyr and SBA-15-NH_2-Tyr (Figure S13) showed C═O and C—N stretching bands at 1700 cm^{-1} and 1430 cm^{-1}, respectively, as well as N—H bending at 1137 cm^{-1} (Table S3), which also suggested the adsorption of the oxidized product L-dopachrome after the catalytic reaction.

With the purpose of analysing the reversibility of the observed adsorption, the SBA-15 and SBA-15-NH_2 obtained after 20 min-interaction with 1 mM oxidized phenols (*i.e.*, dopamine$_{ox}$, DOPA$_{ox}$ and TBC$_{ox}$) were washed with a solution containing citrate (50 mM) and SDS (2 mM). After 3 and 6 washings, the mass losses of the washed solids remained in a range between 27 and 37 wt% (Fig. 6b, grey background), at the same time the presence of phenols or oxidized products could not be detected *via* UV/Vis in the collected supernatants (Figure S11, dashed lines). It was only possible to remove the citrate buffer and SDS adsorbed on the silica after washing three times with water, obtaining mass losses

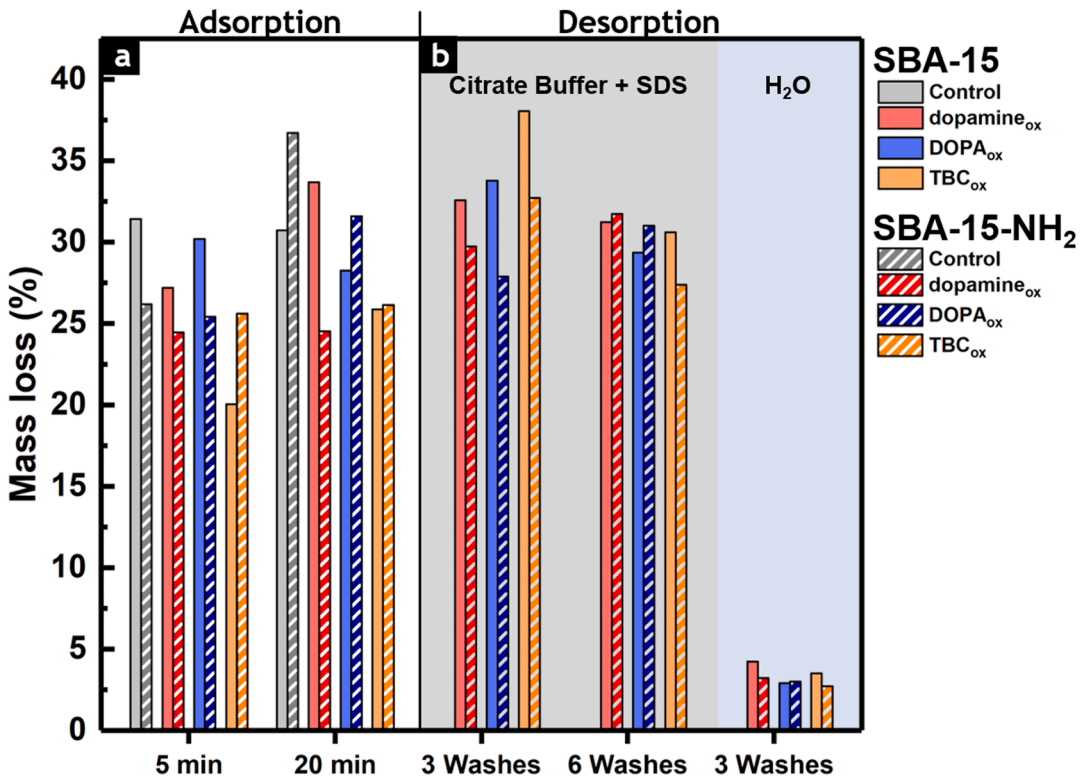

Fig. 6. (a) Adsorption of phenolic compounds on SBA-15 and SBA-15-NH_2 materials. The controls (grey bars) correspond to silica that did not interact with oxidized phenols (1 mM) but only with citrate buffer (50 mM) and SDS (2 mM). (b) Desorption of phenolic compounds from silica after washing the samples with citrate buffer/SDS or only with distilled water. The correspondent mass losses are highlighted with a gray or blue background, respectively. (For interpretation of the references to color in this figure legend, the reader is referred to the web version of this article.)

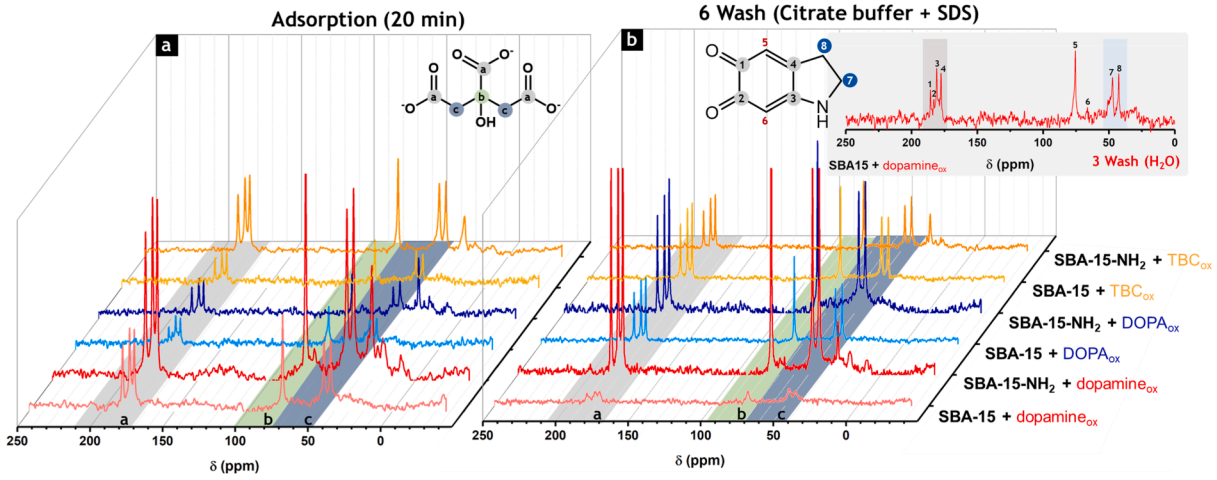

Fig. 7. Solid-state ^{13}C CP/MAS NMR spectra of samples obtained after (a) adsorption experiments and (b) six consecutive washings with citrate buffer and SDS. *Insert:* Solid-state ^{13}C CP/MAS NMR spectra of the SBA-15 washed three times with water after adsorption of oxidized dopamine.

that did not exceed 4 wt% in the washed samples (Fig. 6b, blue background). The effectiveness of water washing in the removal of adsorbed citrate/SDS within the silica pores might have a positive impact on catalysts regeneration and their potential applications in column-type reactors.

3.5. Stability of immobilized AbPPO4 on SBA-15

To evaluate the stability of the immobilized *Ab*PPO4, enzymatic activity tests were performed as described above, but keeping the enzyme-loaded SBA-15 (38 wt% of *Ab*PPO4) at different pH (McIlvaine buffers) or temperature regimes for 1 h before the enzymatic assays. The same concentrations of free *Ab*PPO4 were tested under the same conditions and used as controls (Fig. 8). After 1 h-incubation, activity tests were performed in citrate buffer at pH 6.8 and 25 °C. For the residual enzymatic activities obtained from UV/Vis measurements, the calculated standard deviations were below 5% and corroborate the reproducibility of the experiments performed. The observed gains in enzymatic activity (*i.e.*, 120–130%) with respect to the reference value (i.e., 100% at pH 6.8 and 25 °C) could be attributed to a secondary activation of the latent enzyme. There may be some rearrangements in the C-terminal domain of the protein or a repositioning of the

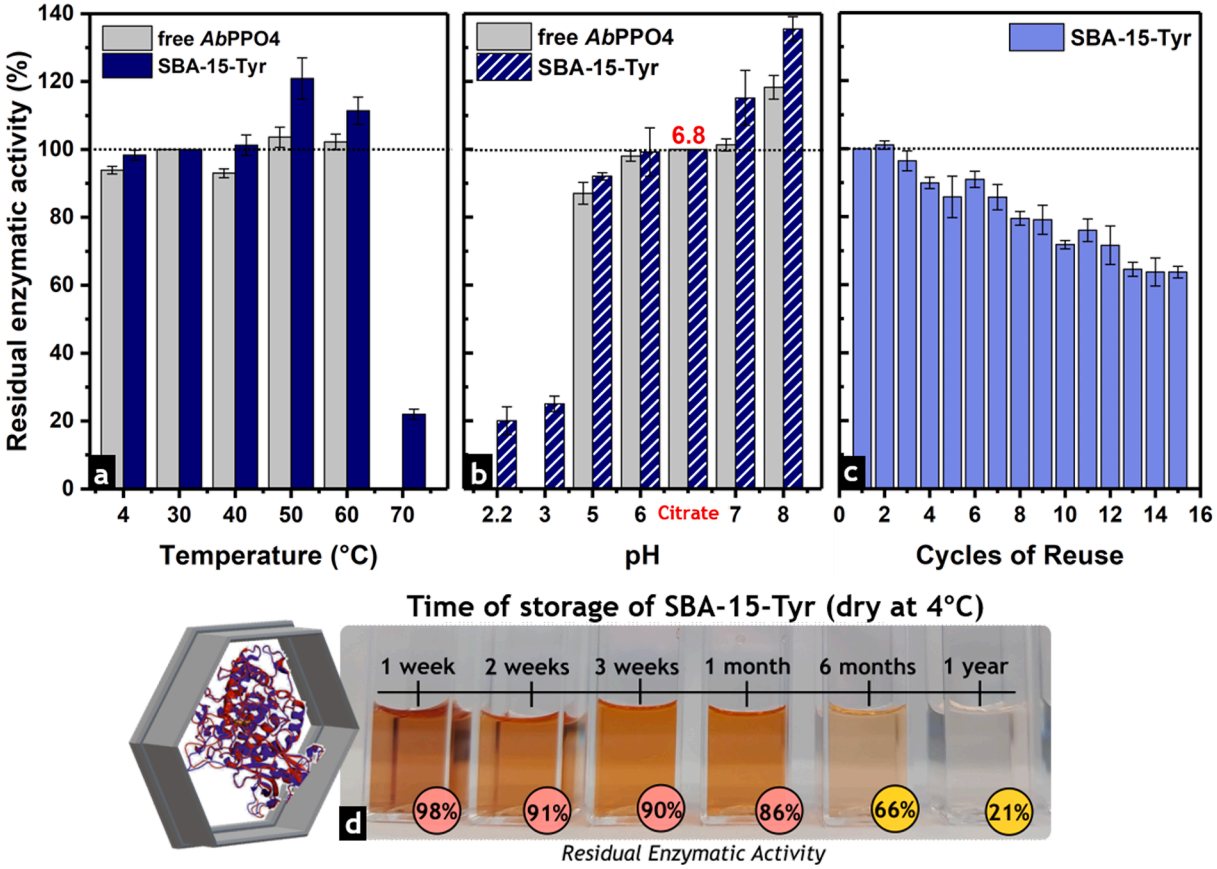

Fig. 8. (a) Effect of temperature on the residual enzymatic activity of SBA-15-Tyr (blue bars) compared to the free enzyme (grey bars). (b) Dependence of the enzymatic activity of SBA-15-Tyr (blue) and free *Ab*PPO4 (grey) on pH. (c) Cycles of reuse of SBA-15-Tyr. (d) Stability of dry SBA-15-Tyr over time. Standard deviation of the residual enzymatic activity data was calculated from triplicates. (For interpretation of the references to color in this figure legend, the reader is referred to the web version of this article.)

immobilized *Ab*PPO4 within the mesopores that allow for slightly better substrate access.[60] The buffer might also influence the enhanced enzymatic activity. For the latent *Dimocarpus longan* PPO, [61] a pronounced increase of enzymatic activity was observed when the enzyme was contacted with 2-(*N*-morpholino)ethanesulfonic acid buffer at 4 °C and then brought back to Tris buffer at room temperature. This could explain the increased activity observed for the immobilized *Ab*PPO4 when the enzyme was transferred from McIlvaine buffers (e.g., pH 7 and 8, 4 °C) to citrate buffer for subsequent measurements of enzymatic activity at standard conditions (25 °C; pH 6.8).

SBA-15-Tyr exhibited enhanced stability over a wide range of pH and temperatures compared to the free *Ab*PPO4, preserving 22%, 20% and 25% of its initial enzymatic activity after keeping the material for 1 h at 70 °C (Fig. 8a), as well as at pH 2.2 and pH 3 (Fig. 8b) respectively, conditions in which the free enzyme was completely deactivated. Strongly acidic pH can cause most tyrosinases to denature, e.g., the activated *Ab*PPO4 retains>50% of its activity at the optimal pH 6.8 only in the pH-range from 5 to 10, but precipitates at pH values below 3 [14], while our studies showed that the latent *Ab*PPO4 is not stable below pH 4.5. These results confirm the advantages of enzyme confinement within the silica pores, which protected *Ab*PPO4 from drastic conditions, expanding the useful range of the catalyst.[62–64]

The stability of SBA-15-Tyr over time was studied by measuring its residual EA several weeks after the immobilization (Fig. 8d) and storage of the dried catalyst at 4 °C. After the first week of storage, the residual EA was found to be 98% of its initial activity. Furthermore, SBA-15-Tyr retained 66% of its initial EA after 6 months and 21% after one year of storage at 4 °C, while the free *Ab*PPO4 was almost completely inactivated at those times (*i.e.*, only 3% of its initial EA was observed). The enzyme-loaded silica could be stored dry at 4 °C, which is only attainable for the free *Ab*PPO4 after lyophilization, but induces the inactivation of the latent enzyme. Such behaviour constituted an important improvement in comparison to other reports of tyrosinase immobilized on solid supports or by other methods of immobilization.[59,63,65]

The reusability of SBA-15-Tyr was also studied for 15 consecutive cycles of substrate oxidation/centrifugation/redispersion (Fig. 8c). Residual enzymatic activity after each cycle was determined using L-tyrosine (1 mM) as substrate for the enzyme. After 6 cycles of reutilization, 91% of the initial enzymatic activity of the enzyme-loaded SBA-15 was retained. Under those conditions, the biocatalyst still showed levels of enzymatic activity comparable to free *Ab*PPO4 in solution. The enzymatic activity of SBA-15-Tyr represented 63% of the initial enzymatic activity after 15 consecutive cycles. This decrease was attributed to the stress suffered by the enzyme after each separation step due to the formation of compact aggregates. There is likely also a purely chemical contribution derived from the reactive oxidation products that can also react with various amino acids of the enzyme.[12,66] However, the possibility of reusing the biocatalyst, maintaining high values of residual enzymatic activity, added to its enhanced stability due to the effect of enzyme confinement, point towards the possible use of SBA-15-Tyr for the preparation of a column-type bioreactor to mimic specific processes in the soil and allow structure elucidation of humic-derived iron-complexes.

4. Conclusions

In this study, the tyrosinase *Ab*PPO4 was successfully immobilized on mesoporous SBA-15-type silica. Liquid adsorption proved to be an

effective immobilization method, not only because of its reproducibility, but also due to the encapsulation of high amounts of *Ab*PPO4 within silica mesopores, capable of efficiently hosting the enzyme with minimal risk of desorption. The adsorbed enzyme in amino-functionalized SBA-15-NH_2 showed an enhanced catalytic performance attributed to the effective interaction between the positively charged SBA-15-NH_2 and the confined enzyme. This rendered the efficient oxidation of several phenolic compounds with high conversion values. Using chromatographic and spectroscopic analyses, we could elucidate the products of the catalytic oxidation reactions and also identify the adsorption of citrate ions as a major factor in the apparent drop in enzyme activity after immobilization. However, we demonstrated the reversibility of this undesirable adsorption, as well as the possibility of regenerating the catalyst through continuous washings, retaining enzymatic activity after several catalytic cycles and consequently its high reusability. This work presents comparable results with other reports involving immobilized tyrosinases,[22,52,67,68] with the added benefit of the enhanced pH-stability, thermal stability and stability in time, even under drastic conditions where the free tyrosinase is inactivated. To the best of our knowledge, this is the first report where the latent *Ab*PPO4 is confined within silica mesopores. In turn, the supported *Ab*PPO4-silica system would represent an accurate model for the construction of column-type bioreactors. Additional studies like enzyme inhibition and interferences in soil samples are currently being planned. Further developments of the proposed methodology may include the enzyme confinement in other mesoporous carriers (*i.e.*, KIT-6-type silica or magnetic metal–organic frameworks) in order to extend the range of applications of the immobilized *Ab*PPO4.

CRediT authorship contribution statement

Claudia Iriarte-Mesa: Conceptualization, Data curation, Formal analysis, Investigation, Methodology, Writing – original draft. **Matthias Pretzler:** Investigation, Data curation, Formal analysis, Writing – review & editing. **Cornelia von Baeckmann:** Formal analysis, Writing – review & editing. **Hanspeter Kählig:** Formal analysis, Writing – review & editing. **Regina Krachler:** Conceptualization, Validation, Writing – review & editing. **Annette Rompel:** Conceptualization, Validation, Supervision, Writing – review & editing, Resources, Funding acquisition. **Freddy Kleitz:** Conceptualization, Supervision, Validation, Writing – review & editing, Resources, Funding acquisition.

Declaration of Competing Interest

The authors declare that they have no known competing financial interests or personal relationships that could have appeared to influence the work reported in this paper.

Data availability

Data will be made available on request.

Acknowledgements

The authors thank the University of Vienna (Austria) and the Austrian Science Research Fund (FWF, P32326 to A.R.) for financial support. The authors thank especially Ms. Anna Fabisikova and the members of the Mass Spectrometry Centre (MSC), Faculty of Chemistry, University of Vienna, for their valuable technical support, precious suggestions and stimulating discussions.

Appendix A. Supplementary data

Supplementary data to this article can be found online at https://doi.org/10.1016/j.jcis.2023.04.158.

References

[1] P.W. Boyd, M.J. Ellwood, The biogeochemical cycle of iron in the ocean, Nat. Geosci. 3 (2010) 675–682, https://doi.org/10.1038/ngeo964.
[2] A. Tagliabue, A.R. Bowie, P.W. Boyd, K.N. Buck, K.S. Johnson, M.A. Saito, The integral role of iron in ocean biogeochemistry, Nature 543 (2017) 51–59, https://doi.org/10.1038/nature21058.
[3] M. Fujii, A. Imaoka, C. Yoshimura, T.D. Waite, Effects of molecular composition of natural organic matter on ferric iron complexation at circumneutral pH, Environ. Sci. Technol. 48 (2014) 4414–4424, https://doi.org/10.1021/es405496b.
[4] G. Sarthou, D. Vincent, U. Christaki, I. Obernosterer, K.R. Timmermans, C.P. D. Brussaard, The fate of biogenic iron during a phytoplankton bloom induced by natural fertilisation: Impact of copepod grazing, Deep, Res. Part II Top. Stud. Oceanogr. 55 (2008) 734–751, https://doi.org/10.1016/j.dsr2.2007.12.033.
[5] E. Ibisanmi, S.G. Sander, P.W. Boyd, A.R. Bowie, K.A. Hunter, Vertical distributions of iron-(III) complexing ligands in the Southern Ocean, Deep, Res. Part II Top. Stud. Oceanogr. 58 (2011) 2113–2125, https://doi.org/10.1016/j.dsr2.2011.05.028.
[6] R. Krachler, R.F. Krachler, Northern High-Latitude Organic Soils As a Vital Source of River-Borne Dissolved Iron to the Ocean, Environ. Sci. Technol. 55 (2021) 9672–9690, https://doi.org/10.1021/acs.est.1c01439.
[7] L.M. Laglera, C. Sukekava, H.A. Slagter, J. Downes, A. Aparicio-Gonzalez, L.J. A. Gerringa, First Quantification of the Controlling Role of Humic Substances in the Transport of Iron across the Surface of the Arctic Ocean, Environ. Sci. Technol. 53 (2019) 13136–13145, https://doi.org/10.1021/acs.est.9b04240.
[8] K.M. Heerah, H.E. Reader, Towards the identification of humic ligands associated with iron transport through a salinity gradient, Sci. Rep. 12 (2022) 15545, https://doi.org/10.1038/s41598-022-19618-2.
[9] A.G. González, A. Bianco, J. Boutorh, M. Cheize, G. Mailhot, A.M. Delort, H. Planquette, N. Chaumerliac, L. Deguillaume, G. Sarthou, Influence of strong iron-binding ligands on cloud water oxidant capacity, Sci. Total Environ. 829 (2022), 154642, https://doi.org/10.1016/j.scitotenv.2022.154642.
[10] F. Panis, A. Rompel, The Novel Role of Tyrosinase Enzymes in the Storage of Globally Significant Amounts of Carbon in Wetland Ecosystems, Environ. Sci. Technol. 56 (2022) 11952–11968, https://doi.org/10.1021/acs.est.2c03770.
[11] F. Panis, R.F. Krachler, R. Krachler, A. Rompel, Expression, Purification, and Characterization of a Well-Adapted Tyrosinase from Peatlands Identified by Partial Community Analysis, Environ. Sci. Technol. 55 (2021) 11445–11454, https://doi.org/10.1021/acs.est.1c02514.
[12] I. Kampatsikas, A. Rompel, Similar but Still Different: Which Amino Acid Residues Are Responsible for Varying Activities in Type-III Copper Enzymes? ChemBioChem 22 (2021) 1161–1175, https://doi.org/10.1002/cbic.202000647.
[13] M. Pretzler, A. Rompel, What causes the different functionality in type-III-copper enzymes? A state of the art perspective, Inorg. Chim. Acta 481 (2018) 25–31, https://doi.org/10.1016/j.ica.2017.04.041.
[14] M. Pretzler, A. Bijelic, A. Rompel, Heterologous expression and characterization of functional mushroom tyrosinase (*Ab*PPO4), Sci. Rep. 7 (2017) 1810, https://doi.org/10.1038/s41598-017-01813-1.
[15] A.M. Mayer, Polyphenol oxidases in plants and fungi: Going places? A review, Phytochemistry 67 (2006) 2318–2331, https://doi.org/10.1016/j.phytochem.2006.08.006.
[16] C. Giulivi, N.J. Traaseth, K.J.A. Davies, Tyrosine oxidation products: Analysis and biological relevance, Amino Acids 25 (2003) 227–232, https://doi.org/10.1007/s00726-003-0013-0.
[17] I. Kipouros, A. Stanczak, J.W. Ginsbach, P.C. Andrikopoulos, L. Rulíšek, E. I. Solomon, Elucidation of the tyrosinase/O_2/monophenol ternary intermediate that dictates the monooxygenation mechanism in melanin biosynthesis, Proc. Natl. Acad. Sci. U. S. A. 119 (2022), https://doi.org/10.1073/pnas.2205619119.
[18] H. Wang, S. Li, J. Li, L. Zhong, H. Cheng, Q. Ma, Immobilized polyphenol oxidase: Preparation, optimization and oxidation of phenolic compounds, Int. J. Biol. Macromol. 160 (2020) 233–244, https://doi.org/10.1016/j.ijbiomac.2020.05.079.
[19] S. Li, L. Zhong, H. Wang, J. Li, H. Cheng, Q. Ma, Process optimization of polyphenol oxidase immobilization: Isotherm, kinetic, thermodynamic and removal of phenolic compounds, Int. J. Biol. Macromol. 185 (2021) 792–803, https://doi.org/10.1016/j.ijbiomac.2021.06.188.
[20] L. Zhong, J. Li, D. Tian, J. Cai, H. Wang, Q. Ma, Immobilization of polyphenol oxidase on chitosan/organic rectorite composites for phenolic compounds removal, Water Sci. Technol. 83 (2021) 906–921, https://doi.org/10.2166/wst.2021.024.
[21] R. Noori, M. Perwez, J.A. Mazumder, J. Ali, M. Sardar, Bio-imprinted magnetic cross-linked polyphenol oxidase aggregates for enhanced synthesis of L-dopa, a neurodegenerative therapeutic drug, Int. J. Biol. Macromol. 227 (2023) 974–985, https://doi.org/10.1016/j.ijbiomac.2022.11.274.
[22] Y.Q. Almulaiky, O. Almaghrabi, Polyphenol Oxidase from *Coleus forskohlii*: Purification, Characterization, and Immobilization Onto Alginate/ZnO Nanocomposite Materials, Catal. Letters 152 (2022) 3089–3099, https://doi.org/10.1007/s10562-022-03916-5.
[23] I.P. Ivanov, L.K. Yotova, Simultaneous immobilization of uricase and peroxidase to copolymer of acrylonitrile with acrylamide, Biotechnol. Biotechnol. Equip. 16 (2002) 104–110, https://doi.org/10.1080/13102818.2002.10819163.
[24] Z. Zhou, M. Hartmann, Recent progress in biocatalysis with enzymes immobilized on mesoporous hosts, Top. Catal. 55 (2012) 1081–1100, https://doi.org/10.1007/s11244-012-9905-0.
[25] C.H. Lee, T.S. Lin, C.Y. Mou, Mesoporous materials for encapsulating enzymes, Nano Today 4 (2009) 165–179, https://doi.org/10.1016/j.nantod.2009.02.001.
[26] D.I. Fried, F.J. Brieler, M. Fröba, Designing Inorganic Porous Materials for Enzyme Adsorption and Applications in Biocatalysis, ChemCatChem 5 (2013) 862–884, https://doi.org/10.1002/cctc.201200640.

[27] M. Hartmann, X. Kostrov, Immobilization of enzymes on porous silicas – benefits and challenges, Chem. Soc. Rev. 42 (2013) 6277–6289, https://doi.org/10.1039/c3cs60021a.
[28] Z. Ashkan, R. Hemmati, A. Homaei, A. Dinari, M. Jamlidoost, A. Tashakor, Immobilization of enzymes on nanoinorganic support materials: An update, Int. J. Biol. Macromol. 168 (2021) 708–721, https://doi.org/10.1016/j.ijbiomac.2020.11.127.
[29] J. Lei, J. Fan, C. Yu, L. Zhang, S. Jiang, B. Tu, D. Zhao, Immobilization of enzymes in mesoporous materials: Controlling the entrance to nanospace, Microporous Mesoporous Mater. 73 (2004) 121–128, https://doi.org/10.1016/j.micromeso.2004.05.004.
[30] M. Kamble, H. Salvi, G.D. Yadav, Preparation of amino-functionalized silica supports for immobilization of epoxide hydrolase and cutinase: characterization and applications, J. Porous Mater. 27 (2020) 1559–1567, https://doi.org/10.1007/s10934-020-00931-y.
[31] A. Costantini, V. Venezia, G. Pota, A. Bifulco, V. Califano, F. Sannino, Adsorption of cellulase on wrinkled silica nanoparticles with enhanced inter-wrinkle distance, Nanomaterials 10 (2020) 1799, https://doi.org/10.3390/nano10091799.
[32] D. Alagöz, N.E. Varan, A. Toprak, D. Yildirim, S.S. Tukel, R. Fernandez-Lafuente, Immobilization of xylanase on differently functionalized silica gel supports for orange juice clarification, Process Biochem. 113 (2022) 270–280, https://doi.org/10.1016/j.procbio.2021.12.027.
[33] J.M. Gómez, M.D. Romero, T.M. Fernández, S. García, Immobilization and enzymatic activity of β-glucosidase on mesoporous SBA-15 silica, J. Porous Mater. 17 (2010) 657–662, https://doi.org/10.1007/s10934-009-9335-y.
[34] H.H.P. Yiu, P.A. Wright, N.P. Botting, Enzyme immobilisation using SBA-15 mesoporous molecular sieves with functionalised surfaces, J. Mol. Catal. Enzym. 15 (2001) 81–92, https://doi.org/10.1016/S1381-1177(01)00011-X.
[35] P. Gholamzadeh, G. Mohammadi Ziarani, A. Badiei, Immobilization of lipases onto the SBA-15 mesoporous silica, Biocatal. Biotransformation 35 (2017) 131–150, https://doi.org/10.1080/10242422.2017.1308495.
[36] K. Wei, X. Wu, B. Ma, Z. Li, Y. Xu, Facile immobilization of his-tagged Microbacterial esterase on Ni-SBA-15 with enhanced stability for efficient synthesis of key chiral intermediate of d-biotin, Bioprocess Biosyst. Eng. 45 (2022) 1075–1088, https://doi.org/10.1007/s00449-022-02729-5.
[37] R. Guillet-Nicolas, F. Bérubé, M. Thommes, M.T. Janicke, F. Kleitz, Selectively tuned pore condensation and hysteresis behavior in mesoporous SBA-15 silica: Correlating material synthesis to advanced gas adsorption analysis, J. Phys. Chem. C 121 (2017) 24505–24526, https://doi.org/10.1021/acs.jpcc.7b06745.
[38] R. Guillet-Nicolas, M. Wainer, L. Marcoux, M. Thommes, F. Kleitz, Exploring the confinement of polymer nanolayers into ordered mesoporous silica using advanced gas physisorption, J. Colloid Interface Sci. 579 (2020) 489–507, https://doi.org/10.1016/j.jcis.2020.05.103.
[39] R. Yildiz, Y. Lorgouilloux, J. Dhainaut, C. Ciotonea, J.P. Dacquin, S. Royer, C. Courtois, Assembly of SBA-15 into hierarchical porous monoliths replicating polymeric scaffolds, Microporous Mesoporous Mater. 337 (2022), https://doi.org/10.1016/j.micromeso.2022.111908.
[40] D.Y. An, W.R. Pu, Y. Wang, Y.P. Xue-Zhang, Z.S.L. Huang, Improving sorption performance of a molecularly imprinted monolithic column by doping mesoporous molecular sieve SBA-15, Microchim. Acta 189 (2022), https://doi.org/10.1007/s00604-022-05192-x.
[41] C. von Baeckmann, R. Guillet-Nicolas, D. Renfer, H. Kählig, F. Kleitz, A Toolbox for the Synthesis of Multifunctionalized Mesoporous Silica Nanoparticles for Biomedical Applications, ACS Omega 3 (2018) 17496–17510, https://doi.org/10.1021/acsomega.8b02784.
[42] T.C. McIlvaine, A buffer solution for colorimetric comparison, J. Biol. Chem. 49 (1921) 183–186, https://doi.org/10.1016/S0021-9258(18)86000-8.
[43] A.M. Schmidt, D.S. Azambuja, E.M.A. Martini, Semiconductive properties of titanium anodic oxide films in McIlvaine buffer solution, Corros. Sci. 48 (2006) 2901–2912, https://doi.org/10.1016/j.corsci.2005.10.013.
[44] S. Brunauer, P.H. Emmett, E. Teller, Adsorption of Gases in Multimolecular Layers, J. Am. Chem. Soc. 60 (1938) 309–319, https://doi.org/10.1021/ja01269a023.
[45] U.K. Laemmli, Cleavage of Structural Proteins during the Assembly of the Head of Bacteriophage T4, Nature 227 (1970) 680–685, https://doi.org/10.1038/227680a0.
[46] D. Kang, Y.S. Gho, M. Suh, C. Kang, Highly sensitive and fast protein detection with Coomassie brilliant blue in sodium dodecyl sulfate-polyacrylamide gel electrophoresis, Bull. Korean Chem. Soc. 23 (2002) 1511–1512, https://doi.org/10.5012/bkcs.2002.23.11.1511.
[47] M. Choi, W. Heo, F. Kleitz, R. Ryoo, Facile synthesis of high quality mesoporous SBA-15 with enhanced control of the porous network connectivity and wall thickness, Chem. Commun. 3 (2003) 1340–1341, https://doi.org/10.1039/b303696k.
[48] M. Thommes, K. Kaneko, A.V. Neimark, J.P. Olivier, F. Rodriguez-Reinoso, J. Rouquerol, K.S.W. Sing, Physisorption of gases, with special reference to the evaluation of surface area and pore size distribution (IUPAC Technical Report), Pure Appl. Chem. 87 (2015) 1051–1069, https://doi.org/10.1515/pac-2014-1117.
[49] S.G. Mauracher, C. Molitor, C. Michael, M. Kragl, A. Rizzi, A. Rompel, High level protein-purification allows the unambiguous polypeptide determination of latent isoform PPO4 of mushroom tyrosinase, Phytochemistry 99 (2014) 14–25, https://doi.org/10.1016/j.phytochem.2013.12.016.
[50] C.N. Pace, F. Vajdos, L. Fee, G. Grimsley, T. Gray, How to measure and predict the molar absorption coefficient of a protein, Protein Science 11 (1995) 2411–2423, https://doi.org/10.1002/pro.5560041120.
[51] K.B. de Oliveira, K.L. Mischiatti, J.D. Fontana, B.H. De Oliveira, Tyrosinase immobilized enzyme reactor: Development and evaluation, J. Chromatogr. B Anal. Technol. Biomed, Life Sci. 945–946 (2014) 10–16, https://doi.org/10.1016/j.jchromb.2013.11.042.
[52] H. Gouzi, T. Moreau, C. Depagne, T. Coradin, Immobilization of a Polyphenol Oxidase Extract from *Terfezia leonis* Tul. Desert Truffle in Multilayered Silica Films for Dopamine Biosensing, Silicon 5 (2013) 241–246, https://doi.org/10.1007/s12633-013-9165-z.
[53] G. Bayramoglu, A. Akbulut, M. Yakup Arica, Immobilization of tyrosinase on modified diatom biosilica: Enzymatic removal of phenolic compounds from aqueous solution, J. Hazard. Mater. 244–245 (2013) 528–536, https://doi.org/10.1016/j.jhazmat.2012.10.041.
[54] L.J.M. Kempkes, J. Martens, J. Grzetic, G. Berden, J. Oomens, Deamidation Reactions of Asparagine- and Glutamine-Containing Dipeptides Investigated by Ion Spectroscopy, J. Am. Soc. Mass Spectrom. 27 (2016) 1855–1869, https://doi.org/10.1007/s13361-016-1462-5.
[55] E. Baltierra-Trejo, L. Márquez-Benavides, J.M. Sánchez-Yáñez, Inconsistencies and ambiguities in calculating enzyme activity: The case of laccase, J. Microbiol. Methods 119 (2015) 126–131, https://doi.org/10.1016/j.mimet.2015.10.007.
[56] J. Yan, G. Pan, L. Li, G. Quan, C. Ding, A. Luo, Adsorption, immobilization, and activity of β-glucosidase on different soil colloids, J. Colloid Interface Sci. 348 (2010) 565–570, https://doi.org/10.1016/j.jcis.2010.04.044.
[57] J. Song, H. Shen, Y. Yang, Z. Zhou, P. Su, Y. Yang, Multifunctional magnetic particles for effective suppression of non-specific adsorption and coimmobilization of multiple enzymes by DNA directed immobilization, J. Mater. Chem. B 6 (2018) 5718–5728, https://doi.org/10.1039/c8tb01842a.
[58] S. Gürdaş, H.A. Güleç, M. Mutlu, Immobilization of *Aspergillus oryzae* β-Galactosidase onto Duolite A568 Resin via Simple Adsorption Mechanism, Food Bioprocess Technol. 5 (2012) 904–911, https://doi.org/10.1007/s11947-010-0384-7.
[59] J. Zdarta, A.S. Meyer, T. Jesionowski, M. Pinelo, Developments in support materials for immobilization of oxidoreductases: A comprehensive review, Adv. Colloid Interface Sci. 258 (2018) 1–20, https://doi.org/10.1016/j.cis.2018.07.004.
[60] Z.L. Yu, W.C. Zeng, X.L. Lu, Influence of ultrasound to the activity of tyrosinase, Ultrason. Sonochem. 20 (2013) 805–809, https://doi.org/10.1016/j.ultsonch.2012.11.006.
[61] L. Ruckthong, M. Pretzler, I. Kampatsikas, A. Rompel, Biochemical characterization of *Dimocarpus longan* polyphenol oxidase provides insights into its catalytic efficiency, Sci. Rep. 12 (2022) 20322, https://doi.org/10.1038/s41598-022-20616-7.
[62] A. Türkhan, E.D. Kaya, A. Koçyiğit, An Innovator Support Material for Tyrosinase Immobilization: Antimony-Doped Tin Oxide Thin Films (ATO-TF), Appl. Biochem. Biotechnol. 192 (2020) 432–442, https://doi.org/10.1007/s12010-020-03337-3.
[63] Y. Wee, S. Park, Y.H. Kwon, Y. Ju, K.M. Yeon, J. Kim, Tyrosinase-immobilized CNT based biosensor for highly-sensitive detection of phenolic compounds, Biosens. Bioelectron. 132 (2019) 279–285, https://doi.org/10.1016/j.bios.2019.03.008.
[64] J. Zdarta, M. Staszak, K. Jankowska, K. Kaźmierczak, O. Degórska, L.N. Nguyen, E. Kijeńska-Gawrońska, M. Pinelo, T. Jesionowski, The response surface methodology for optimization of tyrosinase immobilization onto electrospun polycaprolactone–chitosan fibers for use in bisphenol A removal, Int. J. Biol. Macromol. 165 (2020) 2049–2059, https://doi.org/10.1016/j.ijbiomac.2020.10.081.
[65] A. Hussain, H. Rafeeq, M. Qasim, Z. Jabeen, M. Bilal, M. Franco, H.M.N. Iqbal, Engineered tyrosinases with broadened bio-catalysis scope: immobilization using nanocarriers and applications, 3, Biotech. 11 (2021) 365, https://doi.org/10.1007/s13205-021-02913-6.
[66] C. Iriarte-Mesa, S. Díaz-Castañón, D.G. Abradelo, Facile immobilization of *Trametes versicolor* laccase on highly monodisperse superparamagnetic iron oxide nanoparticles, Colloids Surfaces B Biointerfaces 181 (2019) 470–479, https://doi.org/10.1016/j.colsurfb.2019.05.012.
[67] R. Yavaşer, D. Aktaş Uygun, A.A. Karagözler, Removal of Selected Azo Dyes and Phenolic Compounds via Tyrosinase Immobilized Magnetic Iron Oxide Silver Nanoparticles, Catal. Letters (2022), https://doi.org/10.1007/s10562-022-04087-z.
[68] J. Zeng, G. Du, X. Shao, K.N. Feng, Y. Zeng, Recombinant polyphenol oxidases for production of theaflavins from tea polyphenols, Int. J. Biol. Macromol. 134 (2019) 139–145, https://doi.org/10.1016/j.ijbiomac.2019.04.142.